Received: 26 October 2023 | Accepted: 18 June 2024

DOI: 10.1111/bpa.13283

RESEARCH ARTICLE

Brain Pathology

Intracerebellar administration of the chemokine Cxcl3 reduces the volume of medulloblastoma lesions at an advanced stage by promoting the migration and differentiation of preneoplastic precursor cells

Manuela Ceccarelli[1,2] | **Sabrina Rossi**[3] | **Fabrizio Bonaventura**[4] | **Roberto Massari**[1] | **Annunziata D'Elia**[1] | **Andrea Soluri**[1,5] | **Laura Micheli**[1] | **Giorgio D'Andrea**[1] | **Barbara Mancini**[3] | **Marcello Raspa**[6] | **Ferdinando Scavizzi**[6] | **Rita Alaggio**[3,7] | **Francesca Del Bufalo**[2] | **Evelina Miele**[2] | **Andrea Carai**[8] | **Angela Mastronuzzi**[2] | **Felice Tirone**[1]

[1]Institute of Biochemistry and Cell Biology (IBBC), National Research Council of Italy (CNR), c/o International Campus "A. Buzzati-Traverso", Rome, Italy

[2]Onco-Hematology, Cell Therapy, Gene Therapies and Hemopoietic Transplant, Bambino Gesù Children's Hospital IRCCS, Rome, Italy

[3]Pathology Unit, Bambino Gesù Children's Hospital IRCCS, Rome, Italy

[4]Plaisant Srl, Rome, Italy

[5]Unit of Molecular Neurosciences, University Campus Bio-Medico, Rome, Italy

[6]Institute of Biochemistry and Cell Biology, National Research Council of Italy (IBBC-CNR/EMMA/INFRAFRONTIER/IMPC), c/o International Campus "A. Buzzati-Traverso", Rome, Italy

[7]Department of Medico-surgical Sciences and Biotechnologies, Sapienza University, Rome, Italy

[8]Neurosurgery Unit, Bambino Gesù Children's Hospital IRCCS, Rome, Italy

Correspondence
Manuela Ceccarelli, Onco-Hematology, Cell Therapy, Gene Therapies and Hemopoietic Transplant, Bambino Gesù Children's Hospital IRCCS, Piazza Sant'Onofrio, 4, 00165, Rome, Italy, and Felice Tirone, Institute of Biochemistry and Cell Biology (IBBC), National Research Council of Italy (CNR), c/o International Campus "A. Buzzati-Traverso," Via E. Ramarini, 32, 00015, Monterotondo Scalo(Rome), Italy.
Email: manu.ceccarelli@gmail.com; manuela.ceccarelli@opbg.net and felice.tirone@cnr.it

Funding information
Fondazione Giovanni Celeghin; Fondazione Adriano Buzzati-Traverso; Ministero della Salute; Italian Ministry of Universities and Research

Abstract

The prognosis for many pediatric brain tumors, including cerebellar medulloblastoma (MB), remains dismal but there is promise in new therapies. We have previously generated a mouse model developing spontaneous MB at high frequency, *Ptch1*$^{+/-}$/*Tis21*$^{-/-}$. In this model, reproducing human tumorigenesis, we identified the decline of the Cxcl3 chemokine in cerebellar granule cell precursors (GCPs) as responsible for a migration defect, which causes GCPs to stay longer in the proliferative area rather than differentiate and migrate internally, making them targets of transforming insults. We demonstrated that 4-week Cxcl3 infusion in cerebella of 1-month-old mice, at the initial stage of MB formation, forces preneoplastic GCPs (pGCPs) to leave lesions and differentiate, with a complete suppression of MB development. In this study, we sought to verify the effect of 4-week Cxcl3 treatment in 3-month-old *Ptch1*$^{+/-}$/*Tis21*$^{-/-}$ mice, when MB lesions are at an advanced, irreversible stage. We found that Cxcl3 treatment reduces tumor volumes by sevenfold and stimulates the migration and differentiation of pGCPs from the lesion to the internal cerebellar layers. We also tested whether the pro-migratory action of Cxcl3 favors metastases formation, by xenografting DAOY human MB cells in the

cerebellum of immunosuppressed mice. We showed that DAOY cells express the Cxcl3 receptor, Cxcr2, and that Cxcl3 triggers their migration. However, Cxcl3 did not significantly affect the frequency of metastases or the growth of DAOY-generated MBs. Finally, we mapped the expression of the Cxcr2 receptor in human MBs, by evaluating a well-characterized series of 52 human MBs belonging to different MB molecular subgroups. We found that Cxcr2 was variably expressed in all MB subgroups, suggesting that Cxcl3 could be used for therapy of different MBs.

KEYWORDS
cell migration, Cxcl3 chemokine, Cxcr2 receptor, human biopsies, medulloblastoma, mouse models

1 | INTRODUCTION

Chemokines are a family of low molecular weight (8–14 kDa) cytokines, involved in chemotactic migration and intercellular communication. These secreted proteins are defined by four invariant cysteine residues in their primary amino acid sequence and are classified into four distinct subfamilies (CXC, CC, C, and CX3C) based on the sequence around the first two cysteines [1]. Chemokines bind to specific seven-transmembrane G protein-coupled receptors, classified into four groups (CXCR, CCR, CR, and CX3CR) according to the chemokines they bind, and trigger a wide range of biological responses ranging from cell polarization and movement, to immune and inflammatory responses, angiogenesis, tumor growth, and metastasis [2, 3].

Although chemokines have been identified and extensively studied in the immune system, recent evidence demonstrated the physiological and pathological expression of some of these molecules and their corresponding receptors in the central nervous system (CNS). In the CNS, chemokines are mainly synthesized by astrocytes and microglia and, to a lesser extent by neurons, and represent, after neurotransmitters and neuropeptides, the third major intercellular communication system [4, 5]. In the CNS, chemokines are not only involved in neuroinflammation as mediators of leukocyte infiltration, but also play crucial roles in processes such as development, synaptic transmission, homeostasis, and in neurological disorders associated with severe inflammatory conditions [5, 6]. Most probably, these functions are related to the uneven cerebral distribution of some chemokines and their receptors, which are selectively localized in the hypothalamus, *nucleus accumbens*, limbic system, hippocampus, thalamus, cortex, and cerebellum [4].

The cerebellum has a typical laminated structure composed of three layers, which is the result of the peculiar process of cerebellar development (from the outside to the inside the layers are the molecular layer [ML], the Purkinje cell layer, and the inner granular layer [IGL], respectively). During the postnatal period, cerebellar granule cell precursors (GCPs) proliferate in the external granular layer (EGL) on the cerebellar surface in response to the Sonic Hedgehog (SHH) mitogen secreted by the underlying Purkinje cells. After clonal expansion, GCPs exit the cell cycle, migrate to ML and IGL, and differentiate into mature granule neurons, with disappearance of the EGL and development of the mature three-layered cerebellar structure [7]. In the cerebellum, Purkinje cells and granule neurons co-express multiple functional chemokine receptors and, therefore, are sensitive to a broad range of chemokines [8]. For example, the chemokine Ccl2 is detected in adult and developing cerebellar neurons and plays a neuromodulatory role by influencing the physiological properties of Purkinje cells [9, 10]. Cxcl8, Cxcl1, and Cxcl12 also modulate the activity of cerebellar neurons by enhancing the release of neurotransmitters [11, 12]. Interestingly, the Cxcl12/Cxcr4 axis is crucial for proper cerebellar development: the chemokine Cxcl12 secreted by meninges prevents the premature migration of proliferating GCPs—which express the Cxcr4 receptor—from the EGL, chemoattracting them away from the IGL toward the pia mater overlying the cerebellum [13, 14]. We demonstrated that during cerebellar development the chemokine Cxcl3 exerts an opposite action to Cxcl12, promoting the migration of GCPs from the EGL toward the inner layers [15]. We obtained this result in a new mouse model ($Ptch1^{+/-}/Tis21^{-/-}$) that we have generated by crossing $Ptch1^{+/-}$ mice—spontaneously prone to cerebellar tumorigenesis—with mice lacking the *Tis21* gene, which directly controls the transcription of Cxcl3. In $Ptch1^{+/-}/Tis21^{-/-}$ mice, we observed that downregulation of Cxcl3 expression impairs the GCPs migration outside the EGL, a defect that is rescued by exogenous Cxcl3 administration. Interestingly, in $Ptch1^{+/-}/Tis21^{-/-}$ mice, the delay in the migration of GCPs from the EGL to neighboring layers causes the prolonged permanence of GCPs on the cerebellar surface and their exposure to the proliferative action of SHH, resulting in a dramatic increase of medulloblastoma (MB) frequency [15].

MB is the most common childhood brain tumor and a leading cause of pediatric cancer-related morbidity [16]. MB is a highly heterogeneous disease, with four molecular

subgroups (WNT, SHH, Group 3, and Group 4) of clinical relevance. Each molecular subset arises from peculiar cells of origin and is associated with different genetic alterations, histology, and pathogenesis [16, 17]. Treatment of MB includes maximal safe resection, radio and chemotherapy [18], and causes serious side effects in young patients [19–21]. The development of innovative, more effective and tolerable therapeutic strategies is therefore urgently needed. In this regard, we identified the chemokine Cxcl3 as a MB suppressor, following its administration for 4 weeks by Alzet osmotic minipumps in the cerebellum of 1-month-old *Ptch1*$^{+/-}$/*Tis21*$^{-/-}$ mice [22]. *Ptch1*$^{+/-}$/*Tis21*$^{-/-}$ mice are characterized in the first few months of life by the appearance on the cerebellar surface of regions of ectopic cells, which represent a preneoplastic stage of tumorigenesis [15]. These hyperplastic lesions contain proliferating preneoplastic GCPs (pGCPs), which can give rise to tumors when transplanted but are capable of undergoing migration and differentiation like normal GCPs [23]. We demonstrated that in 1-month-old *Ptch1*$^{+/-}$/*Tis21*$^{-/-}$ mice chronic intracerebellar administration of the chemokine Cxcl3 forces pGCPs to migrate outside the hyperplastic lesions and differentiate, inactivating their neoplastic program and, therefore, leading to the disappearance of MB lesions [22].

In this report, we expand our previous analyses, to test in vivo whether the chemokine Cxcl3 has a migration-promoting action on pGCPs of mice in advanced stages of MB tumorigenesis, preventing the tumor growth. To this aim, we subjected 3-month-old *Ptch1*$^{+/-}$/*Tis21*$^{-/-}$ mice—bearing irreversibly tumor-committed MB lesions—to chronic intracerebellar infusion of the chemokine Cxcl3 by Alzet osmotic minipumps and assessed the presence and extent of MB lesions after 28 days of treatment. Furthermore, to test the therapeutic potential of Cxcl3 in the treatment of human MB, we interrogated a thoroughly characterized series of human MBs belonging to the four molecular subgroups for the expression of the chemokine receptor Cxcr2 and we explored whether the treatment with Cxcl3 increases the risk of metastatic spread by generating an orthotopic MB xenograft model. Indeed, we demonstrated that intracerebellar treatment with Cxcl3 promotes migration and differentiation of pGCPs in 3-month-old *Ptch1*$^{+/-}$/*Tis21*$^{-/-}$ mice, with a highly significant reduction of MB lesions extent, confirming the role of Cxcl3 as a MB suppressor also at a later stage of tumor development. Furthermore, Cxcl3 did not increase the risk of metastasis and could variably act on tumor cells of all MB molecular subgroups, which express the Cxcr2 receptor on their membrane surface. Collectively, these results suggest that the chemokine Cxcl3 may be a potentially relevant molecule for MB therapy.

2 | MATERIALS AND METHODS

2.1 | Mice

Ptch1$^{+/-}$/*Tis21*$^{-/-}$ mice were previously generated [15] by crossing *Ptch1*$^{+/-}$ mice [24] with *Tis21* knockout mice [25], and maintained by continuous inbreeding. Genotyping of *Ptch1*$^{+/-}$/*Tis21*$^{-/-}$ pups was routinely performed by PCR analysis using genomic DNA from tail tips, as described [15].

For in vivo bioimaging studies, 6/7-week-old athymic nude mice (*Foxn1*^{nu}/*Foxn1*$^{+}$) were obtained from the European Mouse Mutant Archive (EMMA; Monterotondo Scalo, Rome, Italy) and housed in individually ventilated mouse cages under controlled conditions (temperature of 22 ± 2°C; relative humidity of 55 ± 15%; 12–15 air changes per hour; 12/12 h light/dark cycle; irradiated standard diet and chlorinated, filtered water ad libitum).

All animal procedures were performed with mice of both sexes, in accordance with the current guidelines of the European Ethical Committee (directive 2010/63/EU) and with the experimental protocol approved by the Italian Ministry of Health (Authorization N. 890/2020-PR).

2.2 | Treatment of *Ptch1*$^{+/-}$/*Tis21*$^{-/-}$ mice and sample preparation

Thirty-six 3-month-old *Ptch1*$^{+/-}$/*Tis21*$^{-/-}$ mice were anesthetized with 2% isoflurane in 100% O_2 through a nose cone and implanted into their cerebellum with an Alzet osmotic minipump, as described [22]. Briefly, an Alzet 30-g infusion cannula (length 1.5 mm; brain infusion kit 3; Durect Corp., Cupertino, CA, USA) was implanted in the subarachnoid space above the rostral, dorsal cerebellum, 5 mm caudal to lambda at midline. The Alzet minipump (1004, which delivers 0.11 μl/h for 4 weeks; Durect Corp.) was filled with recombinant Cxcl3 (100 μl of a solution at 20 μg/ml; 5568-CA-025/CF, R&D Systems, Minneapolis, MN, USA) or with the vehicle (cerebrospinal fluid [CSF] solution, as per Durect Corp. protocol: 148 mM NaCl, 3 mM KCl, 1.4 mM $CaCl_2$, 0.8 mM $MgCl_2$, 8 mM Na_2HPO_4, 0.2 mM NaH_2PO_4) and placed between the scapulas. The cannula was fixed with cyanoacrylate and the skin was closed with sutures. The mice were monitored daily for development of potential neurological deficits and/or distress symptoms until the end of treatment (7 or 28 days). Five days before their sacrifice, mice were injected intraperitoneally with 5-bromo-2′-deoxyuridine (BrdU) (95 mg/kg; Sigma Aldrich, St. Louis, MO, USA) to visualize migrating pGCPs, according to existing protocol [22]. At the end of the treatment, the mice were euthanized under anesthesia by transcardiac perfusion with 4% paraformaldehyde (PFA) in PBS; their cerebella were then dissected, cryoprotected in 30% sucrose in PBS and stored at −80°C until use (i.e., for immunohistochemical studies on MB lesions area and volume and cell migration, proliferation and survival).

2.3 | Immunofluorescence staining, confocal microscopy, and quantification of MB lesions and cell numbers

Immunohistochemical analysis of *Ptch1*$^{+/-}$/*Tis21*$^{-/-}$ cerebella using fluorescent methods was performed as

previously described [22, 26, 27]. Briefly, samples were embedded in Tissue-Tek OCT (Sakura Finetek, Torrance, CA, USA) and cut into 40 μm thick serial free-floating sections on a rotating cryostat at −25°C. To detect the BrdU incorporation, the sections were treated with 2 N HCl 45 min at 37°C and then with 0.1 M sodium borate buffer, pH 8.5, for 10 min. All the samples were permeabilized with 0.3% Triton X-100 in PBS and incubated overnight at 4°C with primary antibodies diluted in 3% normal donkey serum in PBS: a rat monoclonal antibody against BrdU (Abcam, Cambridge, UK; AB6326; 1:300), a mouse monoclonal antibody raised against NeuN (Millipore, Burlington, MA, USA; MAB377; 1:100), a rabbit monoclonal antibody against Ki67 (Thermo Fisher Scientific, Waltham, MA, USA; RM-9106-S1; 1:150), a rabbit polyclonal antibody against cleaved (activated) Caspase3 (Cell Signaling Technology, Danvers, MA, USA; 9661; 1:100), or a rabbit polyclonal antibody against Cxcr2 (Santa Cruz Biotechnology, Santa Cruz, CA, USA; sc-682; 1:200). The following day, the sections were reacted with the appropriate secondary antibodies, diluted in PBS (1:200), all from Jackson ImmunoResearch (West Grove, PA, USA): a donkey anti-rat TRITC-conjugated (BrdU), a donkey anti-mouse conjugated to Alexa-488 (NeuN), or a donkey anti-rabbit Cy3-conjugated (Ki67, Caspase3, Cxcr2). The slices were then counterstained by Hoechst 33258 (1 mg/ml in PBS; Sigma-Aldrich) to visualize the nuclei and the cerebellar layers (i.e., ML and IGL). Photomicrographs of the immunostained sections were collected with an Olympus FV1200 spectral inverted laser scanning confocal microscope and were analyzed by the IAS software (Delta Sistemi, Rome, Italy).

To evaluate the presence of lesions, identified by visualizing the $BrdU^+$ pGCPs, we examined for each cerebellum 12 sagittal sections, at 400 μm of distance, in order to allow a representative sampling. Planimetric measurements of lesion area were performed for the total extension of the lesion in each photomicrograph field by tracing the outline of the whole lesion on the digital picture and were measured with the IAS software. The volume of each lesion was calculated multiplying the average lesion area by section thickness and by number of sections in which the lesion was observed, as described [15].

To quantify pGCPs migrating from the lesions to neighboring layers (i.e., ML and IGL) and differentiating, we analyzed 10 CSF-treated and 9 Cxcl3-treated mice, examining 10 adjacent sagittal sections per lesion. The pGCPs migrating were identified as BrdU-labeled cells in ML and IGL, and counted as percentage ratio to the total number of $BrdU^+$ cells in the lesion and layers, according to a published protocol [22]. Similarly, differentiating pGCPs were identified as $BrdU^+NeuN^+$ cells in ML and IGL, and counted as percentage ratio to the total number of $BrdU^+$ cells in the lesion and layers [22].

Apoptotic (cleaved $Caspase3^+$) or proliferating ($Ki67^+$) cells in lesions of CSF-treated or Cxcl3-treated mice were expressed as a percentage ratio to the total number of cells, labeled by Hoechst 33258, as previously described [26, 27]. The cell counts were performed on about 20–30 randomly representative images, collected under the same parameters from six different lesions for each treatment group.

2.4 | Cell culture and immunocytochemistry

DAOY and D283 cells were cultured in Minimum Essential Medium (MEM; ECB2071L Euroclone, Milan, Italy) [28] and Dulbecco's Modified Eagle's Medium (DMEM; ECM0101 Euroclone) [29], respectively, both medium supplemented with L-glutamine 2 mM, sodium pyruvate 1 mM, 100 U/ml penicillin G, 100 mg/ml streptomycin, and 10% fetal bovine serum (FBS; HyClone, Logan, UT, USA). Cells were maintained in a humidified atmosphere of 5% CO_2 at 37°C.

To visualize Cxcr2 receptor, MB cells were fixed in 4% PFA in PBS for 20 min at RT, permeabilized with 0.1% Triton X-100 in PBS and then incubated for 2 h at RT with the primary rabbit polyclonal antibody against Cxcr2 (Santa Cruz Biotechnology; sc-682; 1:200). The secondary antibody used to visualize the antigen was a donkey anti-rabbit antiserum conjugated to Cy3 (Jackson ImmunoResearch; 1:100). Nuclei were stained by Hoechst 33258 (1 mg/ml in PBS; Sigma-Aldrich). Images of the immunostained cells were obtained by an Olympus FV1200 spectral inverted laser scanning confocal microscope.

2.5 | In vitro migration assay

To analyze the effect of Cxcl3 administration on the in vitro migration of human DAOY and D283 cells we used the scratch wound healing assay, performed as previously described [29–31], with minor modifications. Briefly, DAOY and D283 cells were seeded in 6-well plates at a density of 1×10^5 cells/well and 5×10^5 cells/well, respectively, and grown at 37°C and 5% CO_2 until confluence. Then, a vertical line was made in the cell monolayer with a sterile 1000 μl pipette tip to induce a wound. Scraped off cells were removed by two washes with PBS; fresh medium supplemented with 100 ng/ml of human Cxcl3 (277-GG-010/CF, R&D Systems) or vehicle alone (PBS, 0.1% BSA) was then added to each well, and the cells were maintained at 37°C and 5% CO_2 for the whole duration of the experiment. Images of 4 fields per well were photographed at the time of wound induction (0 h) and 24 h after, using an inverted microscope (Leica DM IRB; Leica Microsystems, Wetzlar, Germany). Wound area was determined by tracing the wound outline on the digital image and measured with IAS software or ImageJ software (National Institutes of Health, USA). The wound healing rate was calculated by comparing the same fields at 0 and 24 h according to the

formula: [(scratch width at 0 h—scratch width at 24 h)/scratch width at 0 h] × 100%. The experiments were repeated twice, with at least three replicates per condition.

To investigate whether the specificity of the pro-migratory effect of Cxcl3 on human DAOY cells depends on binding to the Cxcr2 receptor, a small-molecule inhibitor of Cxcr2 (Reparixin) was used in a scratch wound healing assay to inhibit the Cxcl3 signaling pathway. Reparixin (HY-15251) was purchased from Med Chem Express (Monmouth Junction, NJ, USA) and dissolved in DMSO for storage. The in vitro migration assay was performed as described above, dividing DAOY cells into four groups: cells treated with vehicle alone (0.1% DMSO) for 48 h; cells treated with human Cxcl3 (100 ng/ml) for 48 h; cells treated with Reparixin (100 nM) for 48 h; and cells treated with Reparixin (100 nM) combined with Cxcl3 (100 ng/ml) for 48 h [32]. The experiment was repeated twice, with at least three replicates per condition.

2.6 | Generation of GFP- and Luc-expressing DAOY cell line by lentiviruses infection

To perform the in vivo bioimaging studies, DAOY cell cultures were infected with the lentiviral vector pLL-EF1a-rFLuc-T2A-GFP-mPGK-Puro (System Biosciences, Palo Alto, CA, USA), which expresses both Luciferase and Green Fluorescent Protein, and Puromycin resistance. In DAOY-Luc cells, the GFP was directly visualized by microscopy.

Briefly, the G-glycoprotein vesicular stomatitis virus-pseudotyped lentiviral particles were generated by Calcium Phosphate transfection of HEK293T cells with a 1:2.5 ratio mixture of the pLL-EF1a-rFLuc-T2A-GFP-mPGK-Puro lentiviral vector and the PACKH1 mix containing the three plasmids pGAG, pREV, and pVSV-G. HEK293 cells were cultured in DMEM, supplemented with 10% FBS (HyClone), 100 U/ml penicillin G, and 100 mg/ml streptomycin, at 37°C in 5% CO_2. Then, 4×10^6 cells (50% confluent) were plated in a 10-cm dish 24 h before transfection. Virus-containing medium was harvested 24, 48, and 72 h after transfection and concentrated by two ultracentrifugation steps. The titer of the viral vector was in the range of 10^8 TU/ml. The concentrated virus (1/14 of the virus concentrated from two 10-cm dishes) and polybrene (8 μg/ml; Sigma-Aldrich) were added to DAOY cells 50% confluent in a 35-mm dish containing MEM supplemented with 10% FBS (HyClone), 100 U/ml penicillin G, 100 mg/ml streptomycin, L-glutamine 2 mM, and sodium pyruvate 1 mM, at 37°C in 5% CO_2. After overnight incubation, the procedure of infection of DAOY cells was repeated. DAOY infected cells were then selected with puromycin (2 μg/ml; Sigma-Aldrich) for 5 days. Afterward, the expression of GFP in infected DAOY cells was checked by fluorescence Leica DM IRB inverted microscope (Leica Microsystems), then cells were harvested and cryopreserved in liquid nitrogen for in vivo injection.

The lentiviruses generated were replicant-deficient. Their manipulation was approved by the Italian Ministry of Health (authorization RM/IC/Op2/20/005) and performed using BSL-2 and ABSL-2 containment.

2.7 | Orthotopic MB xenograft mouse model and in vivo bioimaging studies

Generation of an orthotopic intracerebellar DAOY-Luc xenograft model and in vivo bioimaging studies were performed as previously described [33, 34], with minor modifications. Briefly, fourteen 6/7-week-old athymic nude mice (*Foxn1*^{nu}/*Foxn1*$^{+}$) were anaesthetized by inhalation of isoflurane and placed in a stereotactic frame by hooking their incisors onto the frame hold. A small skin incision (length, 1 cm) and a burr hole (diameter, 0.7 mm) were created using a microsurgical drill (Fine Science Tools, Foster City, CA, USA). DAOY-Luc cells (1×10^5) were resuspended in 10 μl PBS and injected slowly through the burr hole into the left cerebellar hemisphere (stereotactic coordinates from bregma: anteroposterior, 6.0 mm; left lateral, 2.1 mm; dorsoventral, 5.0 mm), using a 25-μl, 30-gauge Hamilton syringe (Sigma-Aldrich) that was inserted perpendicular to the cranial surface. The needle was left in its place after completion of injection for additional 2 min; the needle and syringe were then removed, and the skin was closed with sutures. The mice were monitored daily for neurologic symptoms.

Fourteen days after the DAOY-Luc implantation (i.e., once the tumors were established), the mice were imaged and tumor size was evaluated by bioluminescence acquisition using an in vivo imaging system (MILabs Hybrid OI/CT; MILabs, Houten, the Netherlands). For the acquisitions, the mice were anaesthetized by inhalation of isoflurane, and D-luciferin (115144-35-9; GoldBio, St. Louis, MO, USA) (15 mg/ml stock) was intraperitoneally injected (100 μl per 10 g body weight). At 5 min from the luciferin injection, the mice were imaged for 2 min. Several acquisitions were made per mouse until each mouse reached its peak of electron emission. To quantify the bioluminescence, the electron emission (e^-/s) within each area of interest was determined using the MILabs Hybrid OI/CT software (MILabs). The mice then were grouped according to their bioluminescent values and implanted into their cerebellum with Alzet minipumps filled with Cxcl3 or CSF ($n = 7$ mice for each treatment group), as described above. Four total acquisitions (weekly, over a total of 28 days of treatment) near to the peak value for each mouse were analyzed.

2.8 | Immunohistochemistry

Fifty-two human MB biopsies, representative of the four different molecular MB subgroups, were evaluated for

Cxcr2 receptor expression by immunohistochemistry. Immunohistochemistry was carried out on formalin-fixed paraffin-embedded sections using an automated immunostainer (Dako Omnis; Agilent, Santa Clara, CA, USA) with a primary antibody directed against Cxcr2 (Santa Cruz Biotechnology; sc-682; 1:100). The positive controls were obtained by immunohistochemical analysis of human spleen paraffin sections (see The Human Protein Atlas at the link: Tissue Expression of CXCR2—The Human Protein Atlas), while the negative controls were obtained by omitting the primary antibody. The baseline level of cerebellar Cxcr2 expression was also determined by subjecting to immunohistochemical analysis paraffin-embedded sections of a normal human cerebellum, in which we observed weak labeling in 30% of granule neurons (data not shown). Digital images of the immunostained sections were collected with a digital Pathology Scanner (Philips IntelliSite Pathology Solution 3.2; Philips, Amsterdam, the Netherlands) and were blindly analyzed by two independent authors.

Staining for each MB sample was evaluated by assessing both the percentage of positive tumor cells and the staining intensity. As for the percentage of positive cells, the cases were scored as follows: 0 = positivity rate: 0–10%; 1 = positivity rate: 11–25%; 2 = positivity rate: 26–50%; 3 = positivity rate: 51–75%; 4 = positivity rate: 76–100% [35, 36]. As for the intensity, the cases were scored from 0 to 3, as follows: negative as 0, weak as 1, moderate as 2, and strong as 3. The final IHC score was obtained by multiplying the result of the percentage of stained cells by the result of the staining intensity, as described [36]. The individual IHC scores, shown in Figure S4, were grouped according to the MB molecular profile.

All human MB samples were obtained with patient consent and with approval of the Ethical Committee (Authorization N. 730_OPBG_2013).

2.9 | Statistical analysis

The Chi square test was used to compare the MB lesion frequency in CSF-treated mice versus Cxcl3-treated mice (Figure 1B). Numbers of preneoplastic lesions per cerebellum (Figure 1B), lesion areas and volumes (Figure 1D,E), as well as data of migration and differentiation of pGCPs (Figures 2C,E and S1C,D), were calculated as the mean ± the standard error of the mean (SEM) and compared by the Student's *t* test. Also the DAOY and D283 migration rates (Figures 3C,D and S3C) and the BLI increase values (Figure 4D) are expressed as mean ± SEM and compared by the Student's *t* test. The immunofluorescence data of proliferation and apoptosis of MB lesion cells were expressed as percent values (mean% ± SEM; Figure S2B,D): since their distribution may not have equal variance, they were analyzed with the nonparametric Mann–Whitney *U* test, which does not require the assumption of normal distribution. Finally, to compare the IHC scores of the four different MB molecular subgroups (Figure 5B), expressed as mean ± SEM, we used non-parametric tests, namely, the Kruskal–Wallis test to analyze the main effects and the Mann–Whitney *U* test to analyze the simple effects.

All statistical analyses were performed using StatView 5.0 software (SAS Institute, Cary, NC, USA) or Microsoft Office Excel (Microsoft® Excel® for Mac 2011; version 14.7.3; Microsoft Corporation, Redmond, WA, USA). Differences were considered statistically significant at $p < 0.05$.

3 | RESULTS

3.1 | In 4-month-old *Ptch1*$^{+/-}$/*Tis21*$^{-/-}$ mice, the chronic cerebellar treatment with the chemokine Cxcl3 significantly reduces the extent of MB lesions, inducing pGCPs migration and differentiation

To test whether the chemokine Cxcl3 is able to inhibit the development of advanced stages of MB in vivo, we administered Cxcl3 or vehicle (CSF) for 4 weeks by Alzet osmotic minipumps in the cerebellum of 3-month-old *Ptch1*$^{+/-}$/*Tis21*$^{-/-}$ mice, as previously described [22] (Figure 1A). Indeed, in our high frequency SHH-MB mouse model (i.e., *Ptch1*$^{+/-}$/*Tis21*$^{-/-}$) we previously demonstrated that 3 months of age corresponds to a stage in which the incidence of MB lesions exactly matches that of mice developing MB, therefore an age in which the lesions become irreversible [15]. In the previous study by Farioli-Vecchioli et al. [15], we also show representative images of MB lesions in 3-month-old *Ptch1*$^{+/-}$/*Tis21*$^{-/-}$ mice indicating that they are already developed tumors, and the characterization of these lesions for apoptosis and proliferation, with data comparable to those of the present study.

Here, we observed that in 4-month-old *Ptch1*$^{+/-}$/*Tis21*$^{-/-}$ mice, treated with Cxcl3 for 28 days, the percentage of mice presenting cerebellar lesions was 60.0%, whereas it was 66.7% in CSF-treated mice ($p = 0.7215$, χ^2 test; $n = 15$ mice treated with Cxcl3 and $n = 12$ mice treated with CSF). No significant differences were also detected between Cxcl3-treated and CSF-treated mice in the number of MB lesions per cerebellum, resulting 0.60 ± 0.13 in Cxcl3-treated and 0.67 ± 0.14 in vehicle-treated mice ($p = 0.7339$, Student's *t* test) (Figure 1B).

Next, we measured the extent of lesions present in each 4-month-old mouse lesioned ($n = 9$ Cxcl3-treated and $n = 8$ CSF-treated mice). We observed a 4-fold decrease of the area of MB lesions, identified by visualizing the BrdU$^+$ pGCPs (Figure 1C), in 4-month-old *Ptch1*$^{+/-}$/*Tis21*$^{-/-}$ mice treated with Cxcl3 for 28 days compared to the mice treated with vehicle for the same time ($p < 0.0001$, Student's *t* test; Figure 1D).

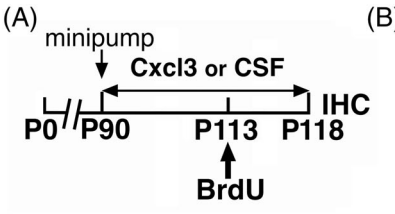

(B)

Treatment	Mice with MB lesions (%, #)		Number of MB lesions per cerebellum (Mean ± SEM)	
28 days in 3-month-old *Ptch1*$^{+/-}$/*Tis21*$^{-/-}$ mice	CSF	Cxcl3	CSF	Cxcl3
	66.7 (8/12)	60.0 (9/15)	0.67 ± 0.14	0.60 ± 0.13
n (mice) analyzed	12	15	12	15
Probability (*p*)	0.7215 (χ^2 test)		0.7339 (Student's *t* test)	

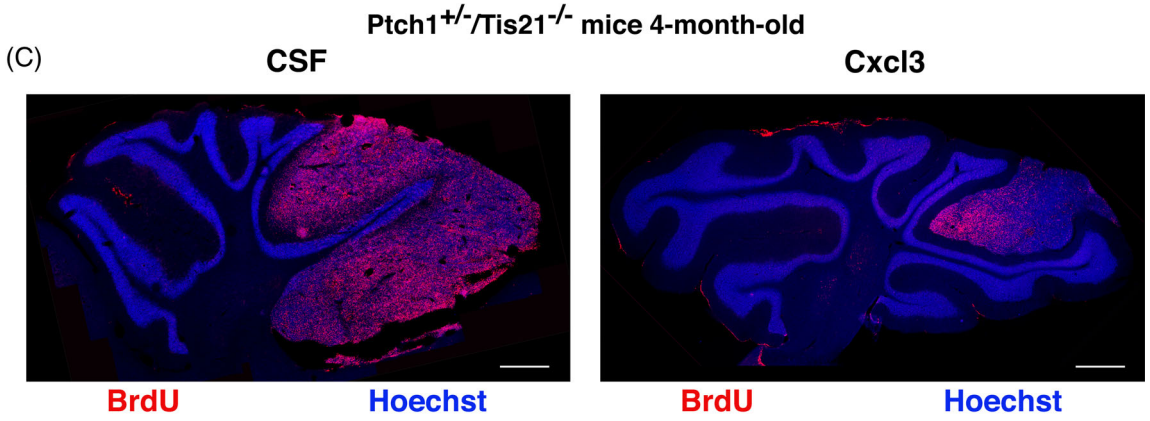

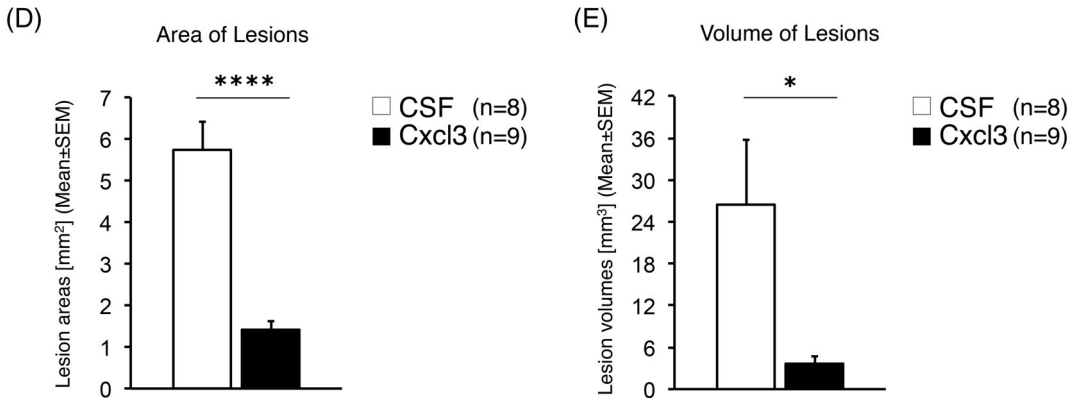

FIGURE 1 Intracerebellar treatment with Cxcl3 dramatically reduces lesion volume in 4-month-old *Ptch1*$^{+/-}$/*Tis21*$^{-/-}$ mice. (A) Treatment timeline: 3-month-old *Ptch1*$^{+/-}$/*Tis21*$^{-/-}$ mice were treated for 28 days with Alzet minipumps filled with recombinant Cxcl3 or vehicle (CSF); a single injection of BrdU was performed 5 days before immunohistochemical analysis. (B) MB lesion frequency and number of preneoplastic lesions per cerebellum in CSF-treated and Cxcl3-treated mice. The number of mice analyzed for each treatment and the statistical analysis are indicated. (C) Representative confocal images of cerebellar sagittal slices of 4-month-old *Ptch1*$^{+/-}$/*Tis21*$^{-/-}$ mice treated with CSF (left) or Cxcl3 (right), respectively. Nuclei were stained with Hoechst 33258 and lesions were identified by the presence of BrdU$^+$ pGCPs (red). Scale bar, 500 μm. (D, E) Bar graphs show the mean ± SEM of lesion areas (D) and lesion volumes (E) measured at the end of 28 days of treatment with Cxcl3 or vehicle. *$p < 0.05$, ****$p < 0.0001$, Student's *t* test; mice analyzed: $n = 8$ for vehicle, $n = 9$ for Cxcl3.

Accordingly, in Cxcl3-treated mice we detected a significant reduction in the volume of MB lesions (sevenfold decrease, $p = 0.0218$, Student's *t* test; Figure 1E) compared to controls (vehicle-treated mice). Overall, these results indicate that intracerebellar treatment for 4 weeks with the chemokine Cxcl3 in mice with MB in advanced stages is not sufficient to fully eradicate the tumor mass, as instead observed in mice with MB in earlier stages [22]; notably, however, they suggest that a longer cerebellar treatment with Cxcl3 could further reduce the MB lesions.

As previously demonstrated [22], in *Ptch1*$^{+/-}$/*Tis21*$^{-/-}$ mice intracerebellar treatment with the chemokine Cxcl3 induces a prolonged period of forced migration of pGCPs from lesions to the neighboring ML and IGL, resulting in terminal differentiation of pGCPs in cerebellar granule neurons. As this process could be responsible for the significant reduction in the extent of MB lesions observed in Cxcl3-treated mice, we analyzed the percentage of pGCPs that migrated outside the lesions and differentiated in 4-month-old *Ptch1*$^{+/-}$/*Tis21*$^{-/-}$ mice treated with Cxcl3 or CSF for 28 days (Figure 2A). pGCPs were double labeled with an injection of BrdU 5 days before analysis and with the differentiation marker NeuN [37] (Figure 2B,D). We observed in Cxcl3-treated mice a highly significant increase in the

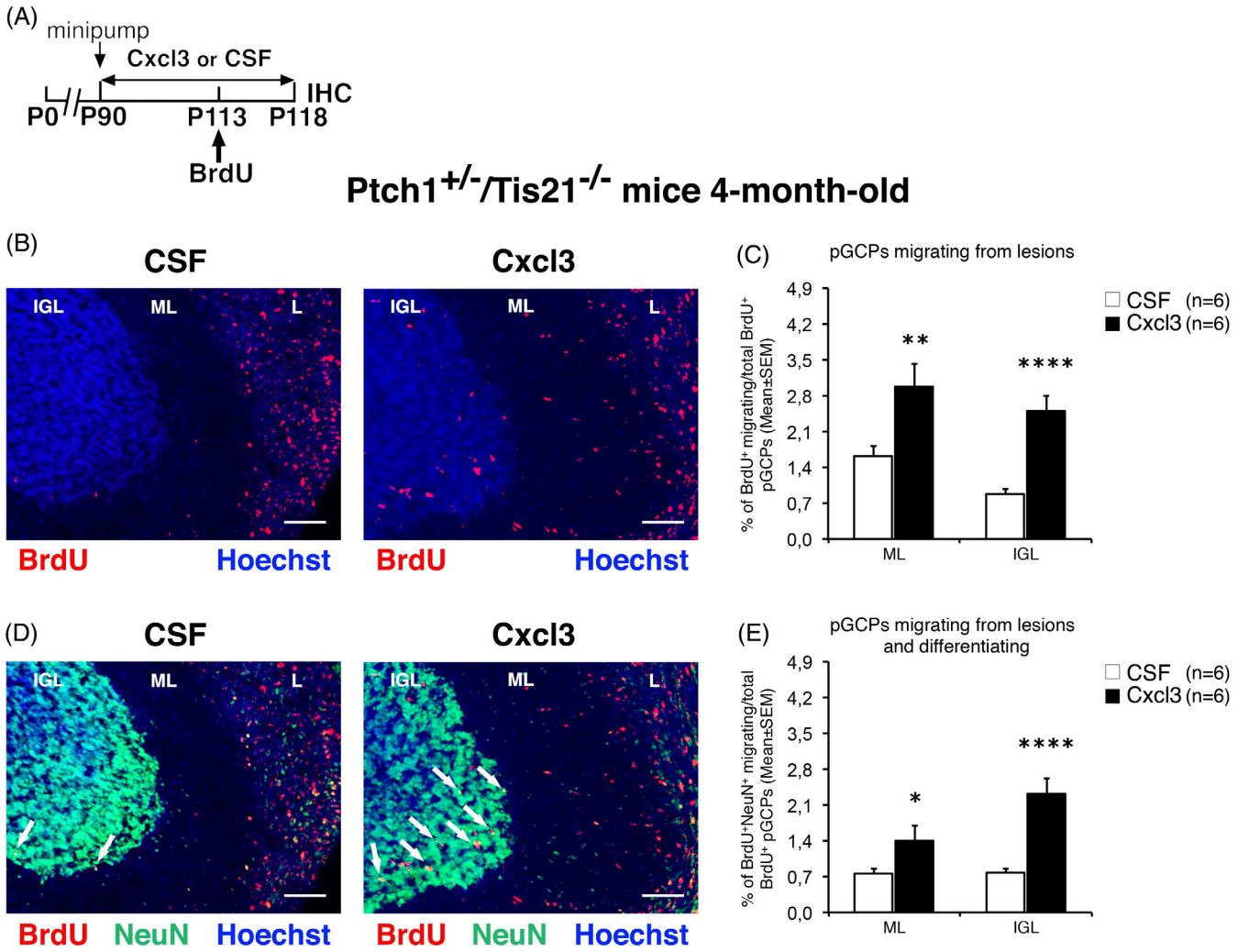

FIGURE 2 In 4-month-old *Ptch1*$^{+/-}$/*Tis21*$^{-/-}$ mice, treatment with Cxcl3 induces neoplastic precursors to migrate from MB lesions to the IGL and differentiate. (A) Experimental timeline: 3-month-old *Ptch1*$^{+/-}$/*Tis21*$^{-/-}$ mice were treated for 4 weeks with Alzet minipumps filled with recombinant Cxcl3 or CSF alone; mice received a single injection of BrdU at P113 and were analyzed by immunohistochemistry at P118. (B) Representative confocal images of pGCPs migrating out of MB lesions, identified as BrdU$^+$ cells (red), in *Ptch1*$^{+/-}$/*Tis21*$^{-/-}$ cerebella chronically treated with CSF or Cxcl3. Sections are counterstained with Hoechst 33258 to visualize the lesion (L), molecular layer (ML), and internal granular layer (IGL). Scale bar, 50 μm. (C) Migrating pGCPs were quantified as percentage ratio (mean ± SEM) of BrdU$^+$ cells present within the ML or IGL area adjacent to each lesion to the total number of BrdU$^+$ cells in the lesion, ML and IGL. **$p < 0.01$, ****$p < 0.0001$, Student's t test; mice analyzed: $n = 6$ for each treatment. (D) The same confocal sections of (B) were also reacted with antibody against NeuN (green), to label migrating and differentiating pGCPs (BrdU$^+$NeuN$^+$). Sections are counterstained with Hoechst 33258 to visualize the lesion, ML and IGL. Scale bar, 50 μm. Some differentiated cells in the IGL are indicated by white arrows. (E) Quantification of the percentage ratio (mean ± SEM) of BrdU$^+$NeuN$^+$ cells present within the ML or IGL area adjacent to each lesion to the total number of BrdU$^+$ cells in the lesion, ML and IGL. * $p < 0.05$, **** $p < 0.0001$, Student's t test; mice analyzed: $n = 6$ for each treatment.

percentage of BrdU$^+$ pGCPs migrating from the lesion to the ML and IGL, compared to vehicle-treated mice (percentage difference of BrdU$^+$/total BrdU$^+$ cells in Cxcl3-treated mice vs. CSF-treated mice, $p = 0.0041$ in ML and $p < 0.0001$ in IGL, Student's t test; Figure 2B,C). In both experimental groups, almost all BrdU$^+$ pGCPs migrating to ML and IGL were terminally differentiated (percentage difference of BrdU$^+$NeuN$^+$/total BrdU$^+$ cells in Cxcl3-treated vs. CSF-treated mice, $p = 0.0299$ in ML and $p < 0.0001$ in IGL, Student's t test; Figure 2D,E). These results indicate that in vivo administration of Cxcl3 in the cerebellum of the high frequency SHH-MB mouse model *Ptch1*$^{+/-}$/*Tis21*$^{-/-}$ is also active in lesions irreversibly committed to developing tumors, exerting potent pro-migratory and differentiative effects on pGCPs.

Despite the highly significant difference we observed in pGCPs migration between Cxcl3-treated and CSF-treated mice, the percentage of BrdU$^+$ migrating cells from the lesion to the inner cerebellar layers in mice treated with Cxcl3 for 4 weeks was low (percentage of BrdU$^+$/total BrdU$^+$ in Cxcl3-treated mice: 2.98 ± 0.45% in the ML and 2.49 ± 0.31% in the IGL). These data represent migration over the last 5 days of treatment and

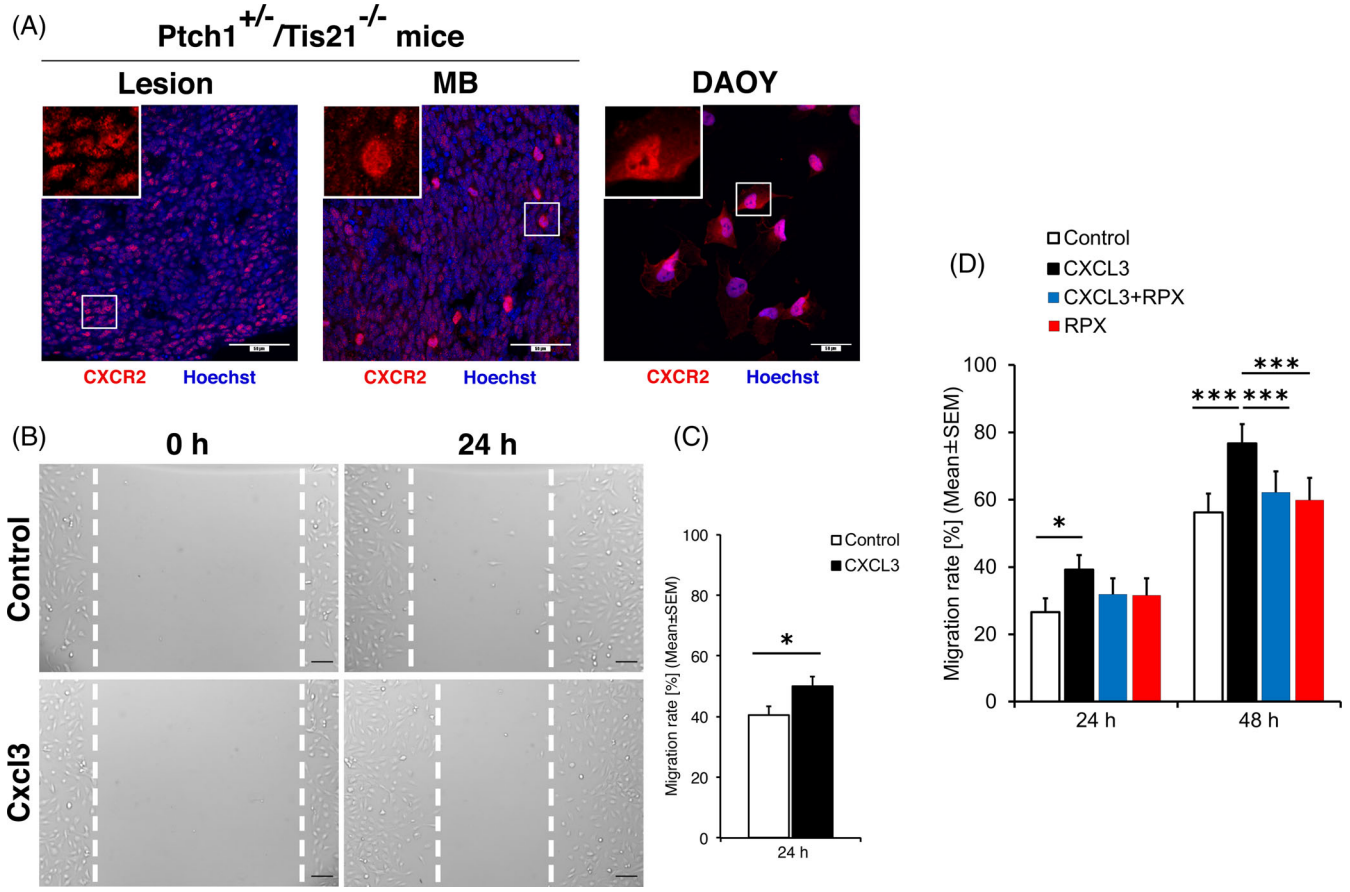

FIGURE 3 Expression of the chemokine receptor Cxcr2 in MB tissue of *Ptch1*$^{+/-}$/*Tis21*$^{-/-}$ mice and DAOY cells. (A) Representative confocal images of Cxcr2^{+} cells (red) in MB lesion (left) and tumor tissue (middle) of *Ptch1*$^{+/-}$/*Tis21*$^{-/-}$ mice, and SHH-type MB cell line DAOY (right). Sections are counterstained with Hoechst 33258 to visualize nuclei. Scale bar, 50 μm. Cells in boxed areas are shown at higher digital magnification (3×). (B) Test of the ability to migrate in response to Cxcl3 of DAOY cells by scratch wound healing assay. Representative photomicrographs of DAOY cells (magnification 4×; scale bar 500 μm) taken at time of scraping (0 h) and 24 h after treatment with 0.1% BSA (as control; top) or Cxcl3 (bottom). Dashed white lines indicate wound boundaries. (C) Mean ± SEM of migration rate calculated as reported in the Materials and Methods section 24 h after wound scratching in control or Cxcl3-treated DAOY cells. (D) Quantification of migration rate, expressed as mean ± SEM, 24 and 48 h after wound scratching in DAOY cells treated with vehicle alone (white bars), with the chemokine Cxcl3 (black bars), with Reparixin (Rpx, red bars), or with the combination Cxcl3 + Rpx (blue bars), respectively. (C, D) Data were obtained from two separate experiments, counting approximately four fields per well (at least three wells per experiment). *$p < 0.05$, ***$p < 0.001$, Student's *t* test.

underestimate the overall migration over the 28 days of implantation of the Alzet minipump, with probable migratory burst at the start of treatment. To test this hypothesis, nine *Ptch1*$^{+/-}$/*Tis21*$^{-/-}$ mice were sacrificed 7 days after Alzet minipump implantation, then analyzed by immunohistochemistry to measure the percentage of pGCPs migrating out of the lesions and differentiating (Figure S1A). In lesioned mice previously treated with Cxcl3 for 7 days we observed a significantly higher percentage of BrdU^{+} pGCPs migrating from the lesion to the ML and IGL compared to lesioned mice treated for 1 week with vehicle alone (percentage difference of BrdU^{+}/total BrdU^{+} cells in Cxcl3-treated mice vs. CSF-treated mice, $p < 0.0001$ in ML and IGL, Student's *t* test; Figure S1B,C). This highly significant difference between mice treated with Cxcl3 or CSF for 7 days is also observed in the percentage of BrdU^{+} pGCPs migrating to ML and IGL that are terminally differentiated (percentage difference of BrdU^{+}NeuN^{+}/total BrdU^{+} cells in Cxcl3-treated vs. CSF-treated mice, $p < 0.0001$ in ML and IGL, Student's *t* test; Figure S1B,D). Noteworthy, the effect of Cxcl3 administration on the migration of pGCPs from the MB lesion toward the internal layers and on the differentiation of pGCPs is significantly more pronounced in the first week than at the end of 28 days of treatment (percentage difference of BrdU^{+}/total BrdU^{+} cells in mice treated with Cxcl3 for 7 days vs. mice treated with Cxcl3 for 28 days, for ML: 4.18-fold increase and $p < 0.0001$; for IGL: 1.76-fold increase and $p = 0.00031$; percentage difference of BrdU^{+}NeuN^{+}/total BrdU^{+} cells in mice treated with Cxcl3 for 7 days vs. mice treated with Cxcl3 for 28 days, for ML: 6.63-fold increase and $p < 0.0001$; for IGL: 1.57-fold increase and $p = 0.00620$; Student's *t* test): this suggests that the prolonged pro-migratory action of Cxcl3 is the main responsible for the reduction of tumor extension.

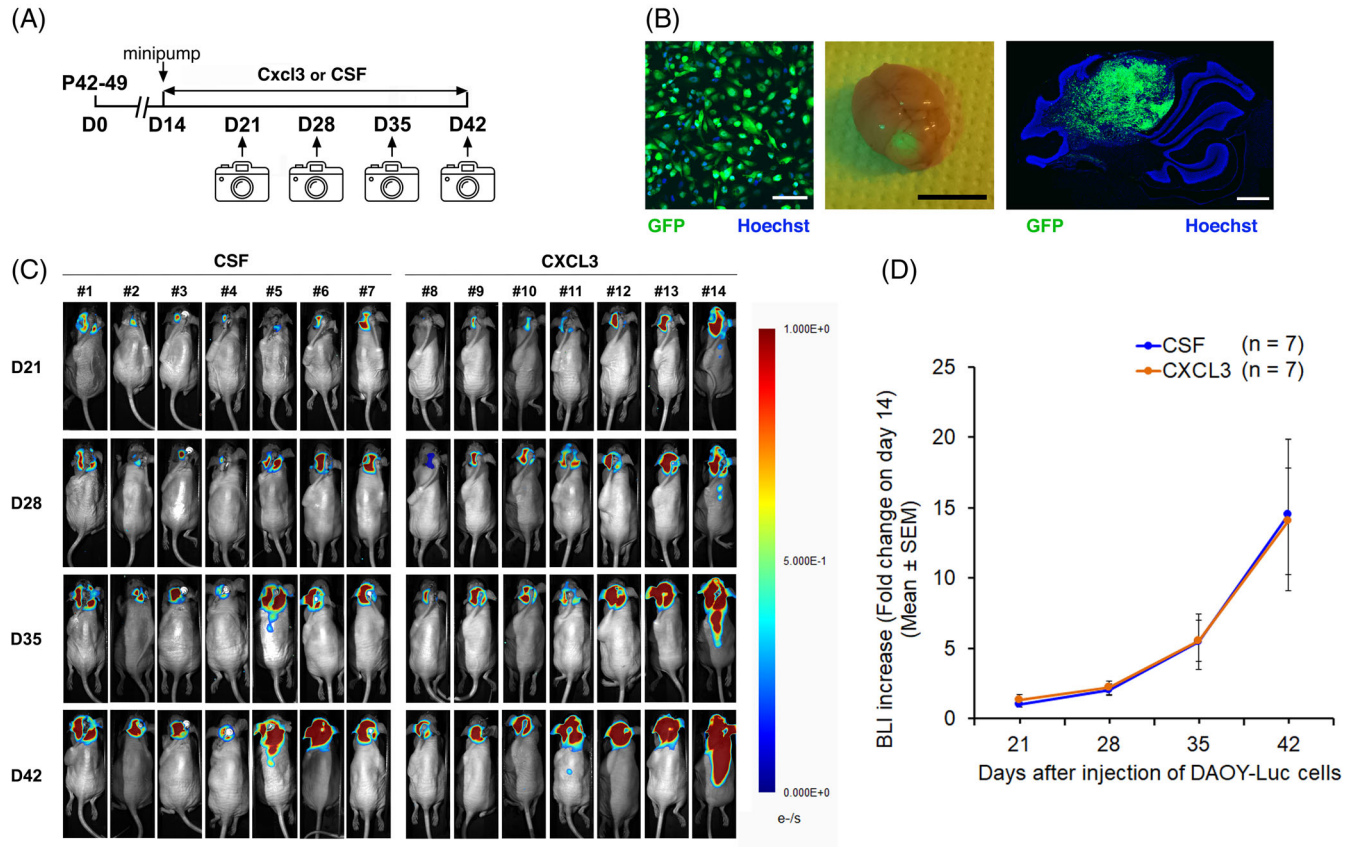

FIGURE 4 In vivo imaging of an orthotopic xenograft mouse model obtained by intracerebellar implantation of engineered human DAOY MB cells. (A) Treatment timeline: Six/seven-week-old athymic nude mice (*Foxn1*^{nu}/*Foxn1*$^{+}$) were implanted into the left cerebellar hemisphere with 1×10^5 human DAOY MB cells engineered to express GFP and firefly Luciferase (FLuc) genes (D0); 14 days after cell grafting (D14), mice were grouped according to their bioluminescence values and implanted with Alzet minipumps filled with recombinant Cxcl3 or CSF. During 4 weeks of treatment, mice were imaged every 7 days (D21, 28, 35, and 42) via in vivo bioluminescent imaging to monitor tumor growth and spinal cord metastases. (B) Left: DAOY cells, infected with a lentiviral vector encoding GFP-FLuc, express GFP in vitro as determined by confocal fluorescence imaging (green cells; nuclei were stained with Hoechst 33258). Middle: DAOY cells implanted in the cerebellum of nude mice give rise to large intracerebellar tumors, as visible by illuminating the explanted brains at the end of treatment with a "GFP flashlight" (Nightsea) which causes GFP^{+} tumors to glow. Right: Representative image by confocal microscopy of a cerebellar sagittal slice obtained from the brain shown in the middle image, showing MB cells, identified as GFP^{+} cells (in green), 42 days after intracerebellar injection of engineered DAOY cells. The section is counterstained with Hoechst 33258 to visualize the ML and granule neurons in the IGL. Scale bars, 100 μm (left), 1 cm (middle), and 600 μm (right). (C) Representative bioluminescence images of nude mice orthotopically injected with DAOY-Luc MB cells and after 14 days implanted with Alzet minipumps filled with CSF or Cxcl3, respectively (7 mice for each treatment group). Images are shown for days 21, 28, 35, and 42 after injection of DAOY-Luc cells. Three animals, one CSF-treated mouse (#5) and two Cxcl3-treated mice (#11 and #14), developed metastases during the 28 days of Alzet implantation. (D) Tumor growth according to quantified electron emission (e^{-}/s) from the cerebellar region of mice injected with DAOY-Luc cells and treated in vivo for 4 weeks with Cxcl3 (orange) or CSF as vehicle (blue). The filled circles and the error bars indicate the mean ± SEM of the bioluminescence imaging (BLI) increase measured at the days of treatment indicated with respect to the day of Alzet implantation (D14). $p = 0.4124$ at D21, $p = 0.8462$ at D28, $p = 0.9867$ at D35, $p = 0.9500$ at D42, Student's t test.

However, it cannot be excluded that some other cellular mechanism, such as the proliferation and/or survival of pGCPs, may influence the extent of the lesions. Therefore, we investigated the cellular parameters of pGCPs in preneoplastic lesions of Cxcl3-treated or vehicle-treated mice by immunohistochemistry, as described [26]. To verify the effect of Cxcl3 on pGCPs apoptosis and proliferation, we measured the percentage of cells labeled with antibodies against cleaved Caspase3 [38] or Ki67 [39], respectively, within MB lesions of 4-month-old *Ptch1*$^{+/-}$/*Tis21*$^{-/-}$ mice previously treated with Cxcl3 or CSF for 28 days (Figure S2). We observed that in Cxcl3-treated mice the percentage of apoptotic pGCPs was significantly lower than in control mice (percentage of Caspase3^{+}/total cells in Cxcl3-treated vs. CSF-treated mice, $p < 0.0001$, Mann–Whitney U test; Figure S2A,B), while no difference in proliferation was found between the two experimental groups (percentage of Ki67^{+}/total cells in Cxcl3-treated vs. CSF-treated mice, $p = 0.4164$; Mann–Whitney U test; Figure S2C,D). The latter result is in agreement with previously reported data indicating that administration of the chemokine Cxcl3 does not affect cerebellar granule proliferation [15].

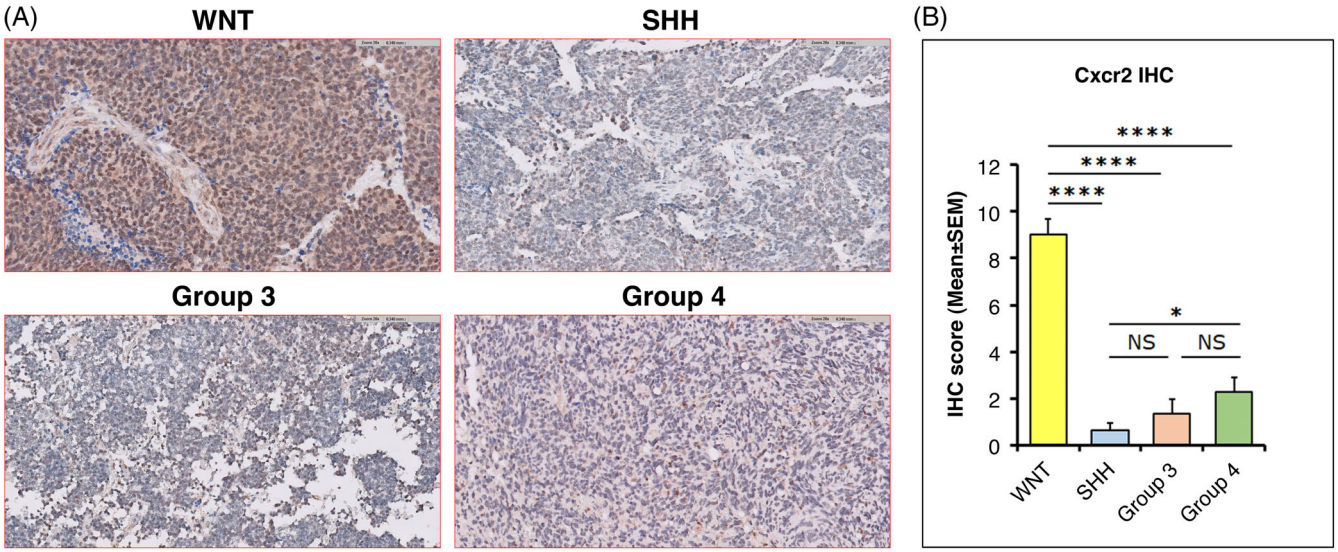

FIGURE 5 Expression of the chemokine receptor Cxcr2 in human medulloblastomas. (A) Representative images of immunohistochemical staining of the chemokine receptor Cxcr2 in human MBs belonging to the 4 molecular subgroups of medulloblastoma (WNT, SHH, Group 3, and Group 4), photographed with a digital Pathology Scanner at 20× magnification. Cells expressing Cxcr2 protein are identified by immunoperoxidase staining (brown). Sections are counterstained with hematoxylin to visualize the nuclei. Scale bars are reported in the images. (B) Mean ± SEM of Cxcr2 immunohistochemical expression scores (IHC scores) in human MB molecular subgroups calculated as reported in the Materials and Methods section. Main effect analysis: Kruskal–Wallis test, H value 31.29, p value <0.0001. Simple effects analysis: *$p < 0.05$, ****$p < 0.0001$, NS not significant, Mann–Whitney U test. MBs analyzed: $n = 12$ for the WNT subgroup; $n = 14$ for the SHH subgroup; $n = 15$ for the Group 3 subgroup; $n = 11$ for the Group 4 subgroup. The complete list of samples analyzed with the IHC score of each is shown in Figure S4.

Overall, these results seem to confirm the role of pGCPs migration from lesions to the inner cerebellar layers as the mechanism responsible for the significant reduction of lesion extent in the high frequency SHH-MB *Ptch1*$^{+/-}$/*Tis21*$^{-/-}$ mouse model chronically treated with the chemokine Cxcl3.

3.2 | Human DAOY and D283 MB cells express the chemokine receptor Cxcr2 and migrate in response to Cxcl3 treatment in vitro

We next sought to understand whether the chemokine Cxcl3 is able to stimulate the migration of human MB tumor cells as well. By analogy with our mouse model *Ptch1*$^{+/-}$/*Tis21*$^{-/-}$ recapitulating the biology of SHH-activated MB [15], we conducted in vitro experiments on a metastatic MB cell line derived from a human desmoplastic histotype and mimicking the in vivo expression profiles of human SHH-type MBs, that is, DAOY MB cell line [40–42]. Furthermore, to test whether Cxcl3 can be effective in non-SHH human tumors, we also performed in vitro experiments on D283 cells. The D283 cell line was established from a peritoneal metastasis of a 6-year-old Caucasian child with metastatic MB and is classified as Group 3/4 [40, 43].

First, we verified by immunofluorescence the expression of the chemokine receptor Cxcr2 on the membrane surface of DAOY and D283 cells. As shown in Figures 3A (right) and S3A, the Cxcr2 chemokine receptor is located on the plasma membrane, and additionally in the nucleoplasm (see The Human Protein Atlas at the link: Subcellular localization of CXCR2—The Human Protein Atlas), of all DAOY and D283 cells, albeit with large intracellular variations in protein expression level. The same results were obtained by subjecting sections of MB lesions and tumors from *Ptch1*$^{+/-}$/*Tis21*$^{-/-}$ mice to immunofluorescence analysis of Cxcr2 expression (Figure 3A, left and middle): this suggests that DAOY and D283 cells, similarly to preneoplastic and tumor GCPs of our MB mouse model, may respond to Cxcl3 treatment by increasing their migration.

Next, we analyzed the effect of Cxcl3 administration on in vitro migration of human DAOY and D283 cells using the wound migration assay, which allows testing a durable effect of the chemokine on cell migration. This assay first involved creating a thin "wound" by scratching the cell monolayer with a pipette tip; images of MB cells were then acquired at the beginning and at regular intervals during cell migration to close the wound and compared in order to quantify the cell migration rate (Figures 3B and S3B). In plates containing MB cells treated with Cxcl3, the percentage of wound closure at 24 h post-scratch was significantly higher than in plates containing MB cells treated with vehicle alone (percentage of migration at 24 h DAOY+Cxcl3 vs. DAOY+BSA $p = 0.0102$, Student's t test; Figure 3B,C; percentage of migration at 24 h D283 + Cxcl3 vs. D283 + BSA $p = 0.0137$, Student's t test; Figure S3B,C), demonstrating the ability of these human MB cells expressing the

Cxcr2 receptor on their membrane surface to respond to exogenous Cxcl3 by increasing their migration.

We also confirmed the specificity of Cxcl3 action on DAOY cell migration through binding to the Cxcr2 receptor using the Cxcr2 antagonist Reparixin. Reparixin is an orally available noncompetitive allosteric inhibitor of the chemokine receptors Cxcr1 and Cxcr2, used in several clinical trials due to its good tolerability and safety profile. In agreement with the above results, Cxcl3 treatment significantly increased the ability of DAOY cells to close the wound (percentage of migration DAOY+Cxcl3 vs. DAOY +DMSO: at 24 h $p = 0.0382$, at 48 h $p = 0.0008$, Student's t test; Figure 3D). Combined treatment with Reparixin reduced DAOY cell migration, significantly inhibiting it at 48 h (migration percentage DAOY+Cxcl3 vs. DAOY +Cxcl3 + Rpx: at 48 h $p = 0.0008$, Student's t test; Figure 3D): at this time, the migration percentage of DAOY cells treated with Cxcl3 + Reparixin reached the value observed in cells treated with vehicle alone (migration percentage DAOY+DMSO vs. DAOY+Cxcl3 + Rpx: at 48 h $p = 0.9858$, Student's t test; Figure 3D). Of note, DAOY cells treated with Reparixin alone showed the same migration capacity as untreated cells (percentage of migration DAOY+DMSO vs. DAOY+Rxp: at 24 h $p = 0.4496$, at 48 h $p = 0.3178$, Student's t test; Figure 3D).

Overall, these results suggest that human MB DAOY cells implanted in the mouse cerebellum might respond to intracerebellar treatment with the exogenous chemokine Cxcl3 by migrating from the surface to the inner layers of the cerebellum and differentiating, similarly to what we observed in our spontaneous MB mouse model *Ptch1*$^{+/-}$/*Tis21*$^{-/-}$.

3.3 | In orthotopic MB xenografts obtained by intracerebellar implantation of engineered human MB DAOY cells, chronic treatment with Cxcl3 does not reduce tumor development or increase metastatic dissemination

To verify the latter hypothesis and evaluate the risk of MB metastasis dissemination following Cxcl3 treatment, we generated an orthotopic MB xenograft model by engrafting 6/7-week-old immunosuppressed mice (*Foxn1*^{nu}/*Foxn1*$^{+}$) with metastatic MB DAOY cells, engineered with a lentiviral vector to stably express the GFP and firefly Luciferase (FLuc) genes (Figure 4A). These DAOY-Luc cells express GFP and, when implanted in the cerebellum, give rise to large intracerebellar GFP^{+} tumors with the histopathological features of MB (Figure 4B). More importantly, DAOY-Luc cells express luciferase, an enzyme not expressed endogenously by mammals that oxidizes its substrate luciferin to produce oxyluciferin with subsequent light emission: this phenomenon allows longitudinal monitoring of intracranial tumor growth and response to therapies using in vivo bioluminescence imaging (BLI) [33]. Fourteen days after cell grafting, the mice were randomized into two experimental groups according to their bioluminescence values (luminescence intensity in mice to be treated with Cxcl3 vs. mice to be treated with CSF, $p = 0.3849$, Student's t test; $n = 7$ mice for each treatment group) and implanted into their cerebellum with Alzet minipumps filled with Cxcl3 or vehicle (CSF). During the 28 day-treatment, the size of xenografted MBs and spinal cord metastases in Cxcl3-treated and control-treated immunosuppressed mice were detected weekly by in vivo BLI (Figure 4A).

BLI images were captured at days 21, 28, 35, and 42 after injection of DAOY-Luc cells (Figure 4C) and analyzed for the electron emission from the cerebellar region of interest of each mouse (e^{-}/s/mm^2); BLI signals were then normalized for each mouse to the BLI value obtained on the day of Alzet implantation (D14) to quantify BLI increase and thus tumor growth during 28-day treatment with Cxcl3 or vehicle. We observed that in both experimental groups BLI signals gradually increased during treatment (2- to 2.5-fold increase each week compared to the previous week), with no statistically significant differences in tumor growth between the two treatment groups (Figure 4D). This result was in contrast to what was observed in the mouse model *Ptch1*$^{+/-}$/*Tis21*$^{-/-}$, defective for the cerebellar migration process [15], where the administration of the exogenous chemokine Cxcl3 was able to restore the altered physiological condition, hindering tumor development. It is possible that human MB DAOY cells implanted in a physiologically normal mouse cerebellum behave differently, due to the absence of the tumor niche.

Interestingly, no statistically significant difference was found between CSF-treated and Cxcl3-treated mice also in the spread of metastases ($p = 0.5148$, χ^2 test; Figure 4C), suggesting that exogenous administration of the chemokine Cxcl3 does not result in the risk of this serious side effect.

3.4 | Human MB cells of the four molecular subgroups express the chemokine receptor Cxcr2, albeit with different spread and intensity

To understand whether human MB may respond to Cxcl3 treatment, we evaluated the expression of the chemokine receptor Cxcr2 in 52 human MB biopsies belonging to the four different MB molecular subgroups by immunohistochemistry (Figures S4 and 5A). Staining for each MB sample was assessed by considering both the percentage of positive tumor cells (extent of staining) and the intensity of staining; subsequently, the individual IHC scores, calculated as reported in Section 2, were grouped according to the molecular profile (Figures S4 and 5B).

Our results showed Cxcr2 receptor expression in all MB subgroups, albeit with different spread and intensity.

Notably, we observed no statistically significant differences in Cxcr2 expression between SHH-type MBs and Group 3 tumors ($p = 0.6699$, Mann–Whitney U test; Figure 5B), as well as between Group 3 and Group 4 tumors ($p = 0.0897$, Mann–Whitney U test; Figure 5B), while Group 4 MBs demonstrated significantly higher chemokine receptor expression than SHH-type tumors ($p = 0.0176$, Mann–Whitney U test; Figure 5B). Surprisingly, we observed that the MBs with the highest Cxcr2 receptor expression level belong to the WNT subgroup (Cxcr2 IHC score in WNT-type MBs vs. all other groups, $p < 0.0001$, Mann–Whitney U test; Figure 5B); this is interesting, as this molecular subgroup has the most favorable prognosis and robust therapeutic response to chemotherapy due to the lack of a functional BBB [44].

These results suggest that human MB tumor cells, belonging to the four different molecular subgroups and expressing the Cxcr2 receptor, might respond to intracerebellar treatment with the chemokine Cxcl3. Further studies will be needed to understand whether human MB cells following Cxcl3 treatment migrate in vivo to the inner layers of the cerebellum, resulting in a reduction in tumor extension, in order to consider Cxcl3 administration as a possible therapeutic approach for human MB therapy.

4 | DISCUSSION

Chemokines have been shown to regulate cell migration in leukocytes and in several other cell types including neural cells [6, 45]. We have previously shown that Cxcl3 is expressed post-natally in cerebellar granule neurons where it induces the migration of cerebellar precursors from the EGL to the cerebellar internal layers, that is, ML and IGL [15]. Furthermore, in our *Ptch1*$^{+/-}$/*Tis21*$^{-/-}$ mouse model of high frequency spontaneous MB, Cxcl3 is downregulated, and we showed that exogenous Cxcl3 rescues the defect of migration of GCPs, suggesting that Cxcl3 is responsible for this defect [15]. We confirmed this possibility by showing that Cxcl3 intracerebellar treatment starting at an early stage of MB lesion formation (1 month of age) induces the migration of pGCPs from the EGL to the internal layers where they differentiate, and also prevents tumor formation. This indicates how crucial is the time period that GCPs remain in the EGL under the pro-proliferative transforming influence of SHH [22].

In this study, we tested the possibility to reduce MB lesions at an advanced stage (3 months of age) by stimulating through the chemokine Cxcl3 the pGCPs to migrate out of the MB lesion into the IGL, and to differentiate, thus withdrawing from the neoplastic program. In fact, as mentioned above, we have previously demonstrated that the development of lesions at 1 month of age is completely prevented by intracerebellar treatment with Cxcl3 for 1 month, in association with a significant migration of pGCPs to the IGL, where they differentiate [22]. The percentage of pGCPs migrating and differentiating, after Cxcl3 treatment, is virtually the same (almost 9%), indicating that all the cells that migrate to the internal layers also differentiate, thus exiting from the neoplastic program [22]. By contrast, we show here that the Cxcl3 treatment for 1 month, starting at 3 months of age, that is, when lesions are already formed and are irreversible, is ineffective in altering the frequency of already developed lesions, as expected, but it does strongly reduce the lesion volume, about sevenfold. However, this effect is associated with a lower percentage of MB cells migrating outside the lesion to the IGL, about 2.5%, of which almost 90% differentiate, as assessed by double labeling with BrdU and NeuN. This raises the question whether such a low percentage of migrating cells is sufficient to cause the observed massive decrease of MB volume. We also analyzed the migratory effect from MB lesions in 3-month-old mice 1 week after the beginning of Cxcl3 treatment, when the more active and thus more plastic and responsive MB cells are at the surface of the developing MB lesions, and found that the cell migration from MB lesions is several folds greater than in MB lesions treated with vehicle, with the majority of migrated cells differentiating. This result alone may account for the massive decrease of MB volume exerted by Cxcl3. Additionally, we checked that apoptosis in MB lesions is not increased by Cxcl3 treatment, rather is decreased. This effect may occur because the size of the MB lesion is lower and thus the number of cells in apoptosis, which reside usually at the core of the tumor, is lower. Furthermore, we found that the MB cells inside the lesion do not show changes in proliferation after treatment with Cxcl3. Thus, if we exclude apoptosis and proliferation as variables at the origin of the decreased volume of the lesion, we should also consider that the period of analysis of the migration of MB cells from the lesion spans only one sixth of the period of Cxcl3 treatment (i.e., 5 days after the BrdU injection vs. 30 days of treatment, respectively). This makes reasonable to think that the final outcome of massive reduction of tumor volume is due to the initially very high and then low but continuous MB cell migration, as our data show. Of course, we cannot exclude that other unidentified factors are implicated in the massive MB volume reduction enacted by Cxcl3 treatment.

However, the ability of MB cells to migrate and differentiate, even at an advanced lesion/tumor stage such as at 3 months of age, show that they maintain a level of plasticity, albeit to a reduced level with respect to the earlier MB lesion stage in 1-month-old mice (2.5% vs. 9% of migrating and differentiating cells, respectively). This plasticity is indicated by our observation that almost all the cells migrating from the MB lesion to the IGL do differentiate, thus keeping the features of proliferating pGCPs. In fact, our previous data of 1-month-old high frequency MB mice are in line with the demonstration by Kessler et al. [23] that pGCPs in MB lesions of *Ptch1*

heterozygous mice are still able at that age to migrate and differentiate, although retaining the ability to generate tumors [23, 46], while our present data show that this plastic response is active also at a more developed MB lesion stage. This seems notable, since, as mentioned above, the MB lesions at 3 months of age are irreversible, given that we have observed that at this age the frequency of mice with a lesion is coincident with the frequency of mice developing MB during their life (i.e., 80%) [15]. It would be interesting to test whether MB cells conserve plasticity in the response to Cxcl3 even at their final stage of development, also in the perspective of using Cxcl3 against fully developed tumors.

We also show that the Cxcl3 receptor, Cxcr2, is present in MB lesion cells at an advanced stage and, for the first time by protein detection, that is present in human MBs of different types and also in the human cell lines DAOY and D283, where we demonstrate that Cxcl3 is able to promote cell migration. Cxcr2 is a seven transmembrane G-protein-coupled receptor of chemokines Cxcl1/2/3; ligand binding activates the hydrolysis of phosphoinositide to produce diacylglycerol and inositol 1,4,5-trisphosphate, which in turn activate protein kinase C triggering cellular responses through the mobilization of calcium [47]. Cxcr2 is important for chemotactic migration, which appears to be regulated through receptor endocytosis [48]. Cxcr2 shows restricted expression, in B cells and in neutrophils, and also in the CNS, where is expressed in neurons of the cortex, striatum, thalamus, hypothalamus, and hippocampus [2, 49–51]. In particular, in the cerebellum Cxcr2 ligands appear to increase glutaminergic neurotransmitter release in Purkinje cells and thus modulate neuronal plasticity [52]. Cxcr2 has been observed to be expressed in cancer cells, that is, in lung, colorectal, breast, prostate, ovarian melanoma, pancreatic, and liver cells, where Cxcr2 expression was frequently associated with poor prognosis [53]. Furthermore, it has been recently shown that the inhibition of Cxcr2 in DAOY and D341 Med cells by a chemical antagonist reduces cell proliferation and migration in vitro [54]. These data are compatible with ours, which show that the inhibition of Cxcr2 by the antagonist Reparixin blocks the migratory effect of Cxcl3, and thus indicate that Cxcl3 acts through Cxcr2; however, data by Penco-Campillo et al. [54] lack an evaluation of the effect in vivo, that is, of the peculiar interaction between neural cancer cells and signals coming from the cerebellar niche, which affect the neural plasticity of cancer cells. Moreover, the fact that we do not see effects of Cxcl3 on cerebellar cell proliferation ([15], and this report), suggests that there may be ligand-dependent specific responses to Cxr2 activation (i.e., Cxcl3-specific response). The fact that we find Cxcr2 to be expressed, although with some difference, in all four molecular subgroups of MB would be consistent with the idea that MB precursor cells are embryonically of similar origin. In fact, WNT-activated, Group 3 and Group 4 MBs originate from neural precursor cell of the lower rhombic lip, of the ventricular zone and EGL, and of the upper rhombic lip, respectively (see for review [55]). Similarly, SHH-activated MBs originate from granule neuron precursor cells of the EGL [55]. At any rate, the wide range of Cxcr2 expression in MBs opens the possibility to use Cxcl3 for therapy in all MB types, as also suggested by the pro-migratory effect of Cxcl3 that we observed in the MB Group 3/4 D283 cell line.

We also sought to assess whether the increase of in vivo migration of pGCPs and in vitro migration of MB DAOY cells elicited by Cxcl3 could be associated with an increase of metastases. The *Ptch1* heterozygous MB model develops nondisseminated MBs, which do not generate metastases in the spinal cord after dissemination in the CSF pathways [56]. Thus, we studied this possibility by orthotopic transplantation of Luciferase-expressing DAOY cells in immunosuppressed mice, and followed tumor development by a sensitive luminescence imaging. DAOY cells are considered of SHH-type [40], generate metastases mainly in the spinal cord when implanted in the cerebellum [57], can produce medullospheres (i.e., tumor stem cells) [58] and express more than 97% of MB-associated genes as well as the majority of genes involved in MB metastatization [42]. Metastases conserve the features of the cells of origin, and differ according to MB type (see for review [59]). SHH-type metastases are rarely occurring in first presentation MBs, while in relapses they are more frequent in the site of origin than in leptomeninges and spinal cord [60]. While WNT-type MBs very rarely develop metastases, these are frequent in Group 3 MBs [59]. As a whole, our experiments indicate that no significant increase of DAOY-generated metastases is elicited by Cxcl3 treatment.

However, some considerations are needed. In general, in the development of tumor and/or metastases, niche signals play an important role; for example, the SHH-type MBs show highest level of infiltration of macrophages and T cells. Moreover, MB cells interact heavily with the extracellular matrix (neural interstitial matrix, basal lamina, and perineuronal nets), exchanging signals such as growth factors [59]. Thus, the interaction of endogenous MB lesion cells—developing spontaneously in the 3-month-old *Ptch1* heterozygous mouse—with the surrounding tissues, including the internal cerebellar layers, may differ from the interaction of exogenously transplanted DAOY MB cells. Moreover, the intrinsic plasticity of endogenous MB lesion cells may be greater than that of transplanted MB cells. All these differences in tumor microenvironment may account for the different response to Cxcl3 treatment of DAOY-generated intracerebellar MB, with respect to the in vivo *Ptch1*$^{+/-}$/*Tis21*$^{-/-}$ model, in particular for the lack of decrease in the growth of DAOY-generated MB after Cxcl3 treatment, as indicated by imaging data.

In conclusion, we studied the effect of the chemokine Cxcl3 on SHH-type MB lesions at an advanced and

irreversible stage of development, demonstrating that Cxcl3 strongly inhibits MB development. Further studies will be necessary to test whether the ability of Cxcl3 to induce migration and differentiation of MB cells without increasing the formation of metastases will occur also in patients. We speculate that WNT-activated MBs may be the ideal target for Cxcl3 treatment, considering their high levels of the Cxcl3 receptor expression and the low rates of metastatic dissemination frequency observed in this subset of patients [61]. Another possibility for therapy that we envision is the use of Cxcl3 treatment in conjunction with a CAR-T therapy that selectively eliminates the MB cells escaping Cxcl3 treatment, using for instance ErbB2 as a selective target for T lymphocytes; this target has been already used for CAR-T therapy in the SHH-type MBs [62], also considering that ErbB2 is not expressed in normal brain, which reduces off-target negative effects [62].

AUTHOR CONTRIBUTION

MC: conceptualization, experimental activity, data analysis, made figures, wrote the paper; SR: experimental activity (human biopsies); FB: experimental activity (mice transplants); RM: data analysis (luciferase assays); AD'E: data analysis (luciferase assays); AS: data analysis (luciferase assays); LM: experimental activity (virus generation and production); GD'A: experimental activity (mice maintenance); BM: experimental activity (human biopsies); MR: mice maintenance; FS: mice maintenance; RA: experimental activity (human biopsies); FDB: experimental activity (in vitro studies); EM: experimental activity (human biopsies); AC: surgery (human biopsies); AM: coordinated Bambino Gesù Hospital activities; FT: conceptualization, experimental activity, data analysis, edited figures, wrote the paper. All authors read and approved the final manuscript.

ACKNOWLEDGEMENT

Open access funding provided by BIBLIOSAN. [Correction added on 22 July 2024, after first online publication: BIBLIOSAN funding statement has been added.]

FUNDING INFORMATION

This work was supported by the Fondazione Giovanni Celeghin and from the Fondazione Adriano Buzzati-Traverso (CNR project DSB.AD004.317) to FT. Moreover, this work was supported also by the project Italian Ministry of Universities and Research, and by the Italian Ministry of Health with current research funds.

CONFLICT OF INTEREST STATEMENT

A patent was filed by the National Research Council on the possible use of the chemokine Cxcl3 in medulloblastoma therapy. The authors declare that the research was conducted in the absence of any commercial or financial relationships that could be construed as a potential conflict of interest.

DATA AVAILABILITY STATEMENT

The data described in this report are available within the paper. For patient data analysis, the Cxcr2 receptor expression was performed on 52 primary medulloblastoma samples, which were subtyped into 14 SHH, 12 WNT, 15 Group 3, and 11 Group 4, and are available in Figure S4.

ETHICS STATEMENT

All animal procedures were performed with mice of both sexes, in accordance with the current guidelines of the European Ethical Committee (directive 2010/63/EU) and with the experimental protocol approved by the Italian Ministry of Health (Authorization N. 890/2020-PR). All human medulloblastoma samples were obtained with patient consent (see below) and with approval of the Ethical Committee (Authorization N. 730_OPBG_2013).

PATIENT CONSENT STATEMENT

Informed consent from the parent, legal guardian, or in the case of adult patients, was obtained at the time of the surgical procedure. For minors aged 16 and older, consent to participate in the study was also obtained.

ORCID

Manuela Ceccarelli https://orcid.org/0000-0001-8741-1600
Sabrina Rossi https://orcid.org/0000-0002-1477-8855
Annunziata D'Elia https://orcid.org/0000-0002-5474-5521
Andrea Soluri https://orcid.org/0000-0003-4623-6839
Felice Tirone https://orcid.org/0000-0002-0980-4377

REFERENCES

1. Zlotnik A, Yoshie O. Chemokines: a new classification system and their role in immunity. Immunity. 2000;12:121–7. https://doi.org/10.1016/s1074-7613(00)80165-x
2. Hughes CE, Nibbs RJB. A guide to chemokines and their receptors. FEBS J. 2018;285:2944–71. https://doi.org/10.1111/febs.14466
3. Rossi D, Zlotnik A. The biology of chemokines and their receptors. Annu Rev Immunol. 2000;18:217–42. https://doi.org/10.1146/annurev.immunol.18.1.217
4. Adler MW, Rogers TJ. Are chemokines the third major system in the brain? J Leukoc Biol. 2005;78:1204–9. https://doi.org/10.1189/jlb.0405222
5. Sowa JE, Tokarski K. Cellular, synaptic, and network effects of chemokines in the central nervous system and their implications to behavior. Pharmacol Rep. 2021;73:1595–625. https://doi.org/10.1007/s43440-021-00323-2
6. de Haas AH, van Weering HR, de Jong EK, Boddeke HW, Biber KP. Neuronal chemokines: versatile messengers in central nervous system cell interaction. Mol Neurobiol. 2007;36:137–51. https://doi.org/10.1007/s12035-007-0036-8
7. i Altaba AR, Palma V, Dahmane N. Hedgehog-Gli signalling and the growth of the brain. Nat Rev Neurosci. 2002;3:24–33. https://doi.org/10.1038/nrn704
8. Gillard SE, Lu M, Mastracci RM, Miller RJ. Expression of functional chemokine receptors by rat cerebellar neurons. J Neuroimmunol. 2002;124:16–28. https://doi.org/10.1016/s0165-5728(02)00005-x
9. Meng SZ, Oka A, Takashima S. Developmental expression of monocyte chemoattractant protein-1 in the human cerebellum and

brainstem. Brain Dev. 1999;21:30–5. https://doi.org/10.1016/s0387-7604(98)00065-5
10. van Gassen KL, Netzeband JG, de Graan PN, Gruol DL. The chemokine CCL2 modulates Ca2+ dynamics and electrophysiological properties of cultured cerebellar Purkinje neurons. Eur J Neurosci. 2005;21:2949–57. https://doi.org/10.1111/j.1460-9568.2005.04113.x
11. Giovannelli A, Limatola C, Ragozzino D, Mileo AM, Ruggieri A, Ciotti MT, et al. CXC chemokines interleukin-8 (IL-8) and growth-related gene product alpha (GROalpha) modulate Purkinje neuron activity in mouse cerebellum. J Neuroimmunol. 1998;92:122–32. https://doi.org/10.1016/s0165-5728(98)00192-1
12. Limatola C, Giovannelli A, Maggi L, Ragozzino D, Castellani L, Ciotti MT, et al. SDF-1alpha-mediated modulation of synaptic transmission in rat cerebellum. Eur J Neurosci. 2000;12:2497–504. https://doi.org/10.1046/j.1460-9568.2000.00139.x
13. Ma Q, Jones D, Borghesani PR, Segal RA, Nagasawa T, Kishimoto T, et al. Impaired B-lymphopoiesis, myelopoiesis, and derailed cerebellar neuron migration in CXCR4- and SDF-1-deficient mice. Proc Natl Acad Sci U S A. 1998;95:9448–53. https://doi.org/10.1073/pnas.95.16.9448
14. Zhu Y, Yu T, Zhang XC, Nagasawa T, Wu JY, Rao Y. Role of the chemokine SDF-1 as the meningeal attractant for embryonic cerebellar neurons. Nat Neurosci. 2002;5:719–20. https://doi.org/10.1038/nn881
15. Farioli-Vecchioli S, Cinà I, Ceccarelli M, Micheli L, Leonardi L, Ciotti MT, et al. Tis21 knock-out enhances the frequency of medulloblastoma in Patched1 heterozygous mice by inhibiting the Cxcl3-dependent migration of cerebellar neurons. J Neurosci. 2012;32:15547–64. https://doi.org/10.1523/JNEUROSCI.0412-12.2012
16. Kumar V, Kumar V, McGuire T, Coulter DW, Sharp JG, Mahato RI. Challenges and recent advances in medulloblastoma therapy. Trends Pharmacol Sci. 2017;38:1061–84. https://doi.org/10.1016/j.tips.2017.09.002
17. Northcott PA, Robinson GW, Kratz CP, Mabbott DJ, Pomeroy SL, Clifford SC, et al. Medulloblastoma. Nat Rev Dis Primers. 2019;5:11. https://doi.org/10.1038/s41572-019-0063-6
18. Juraschka K, Taylor MD. Medulloblastoma in the age of molecular subgroups: a review. J Neurosurg Pediatr. 2019;24:353–63. https://doi.org/10.3171/2019.5.PEDS18381
19. Kieffer V, Chevignard MP, Dellatolas G, Puget S, Dhermain F, Grill J, et al. Intellectual, educational, and situation-based social outcome in adult survivors of childhood medulloblastoma. Dev Neurorehabil. 2019;22:19–26. https://doi.org/10.1080/17518423.2018.1424262
20. King AA, Seidel K, Di C, Leisenring WM, Perkins SM, Krull KR, et al. Long-term neurologic health and psychosocial function of adult survivors of childhood medulloblastoma/PNET: a report from the childhood cancer survivor study. Neuro Oncol. 2017;19:689–98. https://doi.org/10.1093/neuonc/now242
21. Moxon-Emre I, Bouffet E, Taylor MD, Laperriere N, Scantlebury N, Law N, et al. Impact of craniospinal dose, boost volume, and neurologic complications on intellectual outcome in patients with medulloblastoma. J Clin Oncol. 2014;32:1760–8. https://doi.org/10.1200/JCO.2013.52.3290
22. Ceccarelli M, Micheli L, Tirone F. Suppression of medulloblastoma lesions by forced migration of preneoplastic precursor cells with intracerebellar administration of the chemokine Cxcl3. Front Pharmacol. 2016;7:484. https://doi.org/10.3389/fphar.2016.00484
23. Kessler JD, Hasegawa H, Brun SN, Emmenegger BA, Yang ZJ, Dutton JW, et al. N-myc alters the fate of preneoplastic cells in a mouse model of medulloblastoma. Genes Dev. 2009;23:157–70. https://doi.org/10.1101/gad.1759909
24. Hahn H, Wojnowski L, Zimmer AM, Hall J, Miller G, Zimmer A. Rhabdomyosarcomas and radiation hypersensitivity in a mouse model of Gorlin syndrome. Nat Med. 1998;4:619–22. https://doi.org/10.1038/nm0598-619
25. Park S, Lee YJ, Lee HJ, Seki T, Hong KH, Park J, et al. B-cell translocation gene 2 (Btg2) regulates vertebral patterning by modulating bone morphogenetic protein/smad signaling. Mol Cell Biol. 2004;24:10256–62. https://doi.org/10.1128/MCB.24.23.10256-10262.2004
26. Ceccarelli M, D'Andrea G, Micheli L, Gentile G, Cavallaro S, Merlino G, et al. Tumor growth in the high frequency medulloblastoma mouse model Ptch1+/-/Tis21KO has a specific activation signature of the PI3K/AKT/mTOR pathway and is counteracted by the PI3K inhibitor MEN1611. Front Oncol. 2021;11:692053. https://doi.org/10.3389/fonc.2021.692053
27. Ceccarelli M, D'Andrea G, Micheli L, Tirone F. Deletion of Btg1 induces Prmt1-dependent apoptosis and increased stemness in Shh-type medulloblastoma cells without affecting tumor frequency. Front Oncol. 2020;10:226. https://doi.org/10.3389/fonc.2020.00226
28. Ceccarelli M, Micheli L, D'Andrea G, De Bardi M, Scheijen B, Ciotti M, et al. Altered cerebellum development and impaired motor coordination in mice lacking the Btg1 gene: involvement of cyclin D1. Dev Biol. 2015;408:109–25. https://doi.org/10.1016/j.ydbio.2015.10.007
29. Onvani S, Terakawa Y, Smith C, Northcott P, Taylor M, Rutka J. Molecular genetic analysis of the hepatocyte growth factor/MET signaling pathway in pediatric medulloblastoma. Genes Chromosomes Cancer. 2012;51:675–88. https://doi.org/10.1002/gcc.21954
30. Abouantoun TJ, MacDonald TJ. Imatinib blocks migration and invasion of medulloblastoma cells by concurrently inhibiting activation of platelet-derived growth factor receptor and transactivation of epidermal growth factor receptor. Mol Cancer Ther. 2009;8:1137–47. https://doi.org/10.1158/1535-7163.MCT-08-0889
31. Pan W, Song XY, Hu QB, Zhang M, Xu XH. TSP2 acts as a suppresser of cell invasion, migration and angiogenesis in medulloblastoma by inhibiting the notch signaling pathway. Brain Res. 2019;1718:223–30. https://doi.org/10.1016/j.brainres.2019.05.004
32. Wen J, Zhao Z, Huang L, Wang L, Miao Y, Wu J. IL-8 promotes cell migration through regulating EMT by activating the Wnt/β-catenin pathway in ovarian cancer. J Cell Mol Med. 2020;24:1588–98. https://doi.org/10.1111/jcmm.14848
33. Asadzadeh F, Ferrucci V, Antonellis PDE, Zollo M. In vivo bioluminescence imaging using orthotopic xenografts towards patient's derived-xenograft medulloblastoma models. Q J Nucl Med Mol Imaging. 2017;61:95–101. https://doi.org/10.23736/S1824-4785.16.02959-9
34. Ferrucci V, de Antonellis P, Pennino FP, Asadzadeh F, Virgilio A, Montanaro D, et al. Metastatic group 3 medulloblastoma is driven by PRUNE1 targeting NME1-TGF-β-OTX2-SNAIL via PTEN inhibition. Brain. 2018;141:1300–19. https://doi.org/10.1093/brain/awy039
35. Catanzaro G, Sabato C, Russo M, Rosa A, Abballe L, Besharat ZM, et al. Loss of miR-107, miR-181c and miR-29a-3p promote activation of Notch2 signaling in pediatric high-grade gliomas (pHGGs). Int J Mol Sci. 2017;18:2742. https://doi.org/10.3390/ijms18122742
36. de Paula Alves Coelho KM, Stall J, Fronza Júnior H, Blasius R, de França PHC. Evaluation of expression of genes CADM1, TWIST1 and CDH1 by immunohistochemistry in melanocytic lesions. Pathol Res Pract. 2017;213:1067–71. https://doi.org/10.1016/j.prp.2017.07.028
37. Weyer A, Schilling K. Developmental and cell type-specific expression of the neuronal marker NeuN in the murine cerebellum. J Neurosci Res. 2003;73:400–9. https://doi.org/10.1002/jnr.10655
38. Porter AG, Jänicke RU. Emerging roles of caspase-3 in apoptosis. Cell Death Differ. 1999;6:99–104. https://doi.org/10.1038/sj.cdd.4400476
39. Scholzen T, Gerdes J. The Ki-67 protein: from the known and the unknown. J Cell Physiol. 2000;182:311–22. https://doi.org/10.1002/(SICI)1097-4652(200003)182:3<311::AID-JCP1>3.0.CO;2-9

40. Ivanov DP, Coyle B, Walker DA, Grabowska AM. In vitro models of medulloblastoma: choosing the right tool for the job. J Biotechnol. 2016;236:10–25. https://doi.org/10.1016/j.jbiotec.2016.07.028
41. Jacobsen PF, Jenkyn DJ, Papadimitriou JM. Establishment of a human medulloblastoma cell line and its heterotransplantation into nude mice. J Neuropathol Exp Neurol. 1985;44:472–85. https://doi.org/10.1097/00005072-198509000-00003
42. MacDonald TJ, Brown KM, LaFleur B, Peterson K, Lawlor C, Chen Y, et al. Expression profiling of medulloblastoma: PDGFRA and the RAS/MAPK pathway as therapeutic targets for metastatic disease. Nat Genet. 2001;29:143–52. https://doi.org/10.1038/ng731
43. Friedman HS, Burger PC, Bigner SH, Trojanowski JQ, Wikstrand CJ, Halperin EC, et al. Establishment and characterization of the human medulloblastoma cell line and transplantable xenograft D283 Med. J Neuropathol Exp Neurol. 1985;44:592–605. https://doi.org/10.1097/00005072-198511000-00005
44. Phoenix TN, Patmore DM, Boop S, Boulos N, Jacus MO, Patel YT, et al. Medulloblastoma genotype dictates blood brain barrier phenotype. Cancer Cell. 2016;29:508–22. https://doi.org/10.1016/j.ccell.2016.03.002
45. Yoneyama M, Shiba T, Hasebe S, Ogita K. Adult neurogenesis is regulated by endogenous factors produced during neurodegeneration. J Pharmacol Sci. 2011;115:425–32. https://doi.org/10.1254/jphs.11r02cp
46. Yang ZJ, Ellis T, Markant SL, Read TA, Kessler JD, Bourboulas M, et al. Medulloblastoma can be initiated by deletion of patched in lineage-restricted progenitors or stem cells. Cancer Cell. 2008;14:135–45. https://doi.org/10.1016/j.ccr.2008.07.003
47. Wu D, LaRosa GJ, Simon MI. G protein-coupled signal transduction pathways for interleukin-8. Science. 1993;261:101–3. https://doi.org/10.1126/science.8316840
48. Rose JJ, Foley JF, Murphy PM, Venkatesan S. On the mechanism and significance of ligand-induced internalization of human neutrophil chemokine receptors CXCR1 and CXCR2. J Biol Chem. 2004;279:24372–86. https://doi.org/10.1074/jbc.M401364200
49. Luan J, Furuta Y, Du J, Richmond A. Developmental expression of two CXC chemokines, MIP-2 and KC, and their receptors. Cytokine. 2001;14:253–63. https://doi.org/10.1006/cyto.2001.0882
50. Semple BD, Kossmann T, Morganti-Kossmann MC. Role of chemokines in CNS health and pathology: a focus on the CCL2/CCR2 and CXCL8/CXCR2 networks. J Cereb Blood Flow Metab. 2010;30:459–73. https://doi.org/10.1038/jcbfm.2009.240
51. Vallès A, Grijpink-Ongering L, de Bree FM, Tuinstra T, Ronken E. Differential regulation of the CXCR2 chemokine network in rat brain trauma: implications for neuroimmune interactions and neuronal survival. Neurobiol Dis. 2006;22:312–22. https://doi.org/10.1016/j.nbd.2005.11.015
52. Lax P, Limatola C, Fucile S, Trettel F, Di Bartolomeo S, Renzi M, et al. Chemokine receptor CXCR2 regulates the functional properties of AMPA-type glutamate receptor GluR1 in HEK cells. J Neuroimmunol. 2002;129:66–73. https://doi.org/10.1016/s0165-5728(02)00178-9
53. Ha H, Debnath B, Neamati N. Role of the CXCL8-CXCR1/2 axis in cancer and inflammatory diseases. Theranostics. 2017;7:1543–88. https://doi.org/10.7150/thno.15625
54. Penco-Campillo M, Molina C, Piris P, Soufi N, Carré M, Pagnuzzi-Boncompagni M, et al. Targeting of the ELR +CXCL/CXCR1/2 pathway is a relevant strategy for the treatment of paediatric medulloblastomas. Cells. 2022;11:3933. https://doi.org/10.3390/cells11233933
55. Azzarelli R, Simons BD, Philpott A. The developmental origin of brain tumours: a cellular and molecular framework. Development. 2018;145:dev162693. https://doi.org/10.1242/dev.162693
56. Wu X, Northcott PA, Dubuc A, Dupuy AJ, Shih DJ, Witt H, et al. Clonal selection drives genetic divergence of metastatic medulloblastoma. Nature. 2012;482:529–33. https://doi.org/10.1038/nature10825
57. Yang WQ, Senger D, Muzik H, Shi ZQ, Johnson D, Brasher PM, et al. Reovirus prolongs survival and reduces the frequency of spinal and leptomeningeal metastases from medulloblastoma. Cancer Res. 2003;63:3162–72.
58. Casciati A, Tanori M, Manczak R, Saada S, Tanno B, Giardullo P, et al. Human medulloblastoma cell lines: investigating on cancer stem cell-like phenotype. Cancers (Basel). 2020;12:226. https://doi.org/10.3390/cancers12010226
59. Van Ommeren R, Garzia L, Holgado BL, Ramaswamy V, Taylor MD. The molecular biology of medulloblastoma metastasis. Brain Pathol. 2020;30:691–702. https://doi.org/10.1111/bpa.12811
60. Ramaswamy V, Remke M, Bouffet E, Faria CC, Perreault S, Cho YJ, et al. Recurrence patterns across medulloblastoma subgroups: an integrated clinical and molecular analysis. Lancet Oncol. 2013;14:1200–7. https://doi.org/10.1016/S1470-2045(13)70449-2
61. Ellison DW, Onilude OE, Lindsey JC, Lusher ME, Weston CL, Taylor RE, et al. Beta-catenin status predicts a favorable outcome in childhood medulloblastoma: the United Kingdom children's cancer study group brain tumour committee. J Clin Oncol. 2005;23:7951–7. https://doi.org/10.1200/JCO.2005.01.5479
62. Nellan A, Rota C, Majzner R, Lester-McCully CM, Griesinger AM, Mulcahy Levy JM, et al. Durable regression of medulloblastoma after regional and intravenous delivery of anti-HER2 chimeric antigen receptor T cells. J Immunother Cancer. 2018;6:30. https://doi.org/10.1186/s40425-018-0340-z

SUPPORTING INFORMATION

Additional supporting information can be found online in the Supporting Information section at the end of this article.

How to cite this article: Ceccarelli M, Rossi S, Bonaventura F, Massari R, D'Elia A, Soluri A, et al. Intracerebellar administration of the chemokine Cxcl3 reduces the volume of medulloblastoma lesions at an advanced stage by promoting the migration and differentiation of preneoplastic precursor cells. Brain Pathology. 2025;35(1):e13283. https://doi.org/10.1111/bpa.13283